HHS Public Access

Author manuscript

Cancer Immunol Res. Author manuscript; available in PMC 2024 May 15.

Published in final edited form as:

Cancer Immunol Res. 2021 July ; 9(7): 748–764. doi:10.1158/2326-6066.CIR-20-0784.

MHC class II antigen presentation by tumoral lymphatics is required for tumor specific signature and suppressive functions of Tregs

Anastasia O. Gkountidi[1,*], **Laure Garnier**[1,*], **Juan Dubrot**[1,2], **Julien Angelillo**[1], **Guillaume Harlé**[1], **Dale Brighouse**[1], **Ludovic J. Wrobel**[3], **Robert Pick**[1], **Christoph Scheiermann**[1,4], **Melody A. Swartz**[5], **Stéphanie Hugues**[1]

[1]Department of Pathology and Immunology, University Medical Center (CMU), Geneva, Switzerland

[2]present address: Broad Institute of Massachusetts Institute of Technology and Harvard, Cambridge, MA, USA

[3]Dermato-Oncology Unit, Division of Dermatology, University Hospital of Geneva, Switzerland.

[4]Walter-Brendel-Centre of Experimental Medicine, University Hospital, Ludwig-Maximilians-University Munich, BioMedical Centre, Planegg-Martinsried, Germany

[5]Ben May Department for Cancer Research, University of Chicago, Chicago, IL, 60637, USA

Abstract

A number of solid malignancies triggers lymphangiogenesis, facilitating metastasis. Recent studies further indicate that tumor-associated lymphatic vessels significantly contribute to the generation of an immunosuppressive tumor microenvironment. Here, we have investigated the ability of tumor-associated lymphatic endothelial cells (LECs) to function as MHC class II restricted antigen-presenting cells in the regulation of anti-tumor immunity. Using murine models of lymphangiogenic tumors engrafted under the skin, we show that tumor LECs upregulate MHCII and the MHCII antigen processing machinery, and promote Treg expansion ex vivo. Using mice with a LEC-restricted lack of MHCII expression, we demonstrate that tumor growth is severely impaired, whereas tumor-infiltrating T effector cells are increased. Reduction of tumor growth and reinvigoration of tumor-specific T cell responses both result from alterations of the tumor-infiltrating regulatory T cell (Treg) transcriptome and phenotype. Treg suppressive functions are consequently profoundly altered in tumors lacking MHCII in LECs. No difference in effector T cell responses or Treg phenotype and functions were observed in tumor-draining lymph nodes, indicating that MHCII restricted antigen presentation by LECs is required locally in the tumor microenvironment (TME) to confer potent suppressive functions to Tregs. Altogether, our study advocates a role for MHCII-restricted antigen-presenting tumor LECs that function as a local brake, dampening tumor T cell immunity and promoting intratumoral Treg suppressive functions.

Correspondence to S. Hugues (stephanie.hugues@unige.ch).
*equal contribution

DISCLOSURE OF POTENTIAL CONFLICTS OF INTEREST
No potential conflicts of interest were disclosed.

Keywords

lymphangiogenic tumors; Treg; antigen-presentation

INTRODUCTION

The TME influences considerably tumor growth and tumor-specific immunity, and is therefore a major regulator of cancer development. The TME is generally a highly immunosuppressed *milieu* due to a vast array of local modifications leading to dysfunctional anti-tumoral adaptive immunity. Among these are alterations in the tumor immune cell infiltrate, with impairment of effector T cells and accumulation of Tregs, promoting tumor growth and cancer cell dissemination [1,2]. Tregs, which establish and maintain immunological tolerance and regulate immune homeostasis [3], are potent suppressors of effector cells and are found at high frequencies in various types of cancers [4,5]. Intratumoral Tregs further undergo a tumor-specific genetic program with respect to different TME [6,7].

The development of several solid tumors triggers angiogenesis and lymphangiogenesis, which consist of expansion and the remodelling of blood and lymphatic endothelial cells (BECs and LECs), respectively. These two complex processes result from the activation of specific tyrosine kinase receptors by vascular endothelial growth factors (VEGFs) and angiopoietin (ANGPTs), which are produced by the tumor itself and tumor infiltrating cells. Tumor-associated (TA) blood vessels provide oxygen and nutrients for tumor cells and, together with lymphatic vessels (LVs), facilitate tumor metastasis [8]. However, the mechanisms by which TA-LVs promote disease progression remains a matter of debate.

LECs express the transcription factor PROX-1, which is essential for their development and maintenance [9], and the surface protein LYVE-1, which is abundant in lymphatic junctions, expressed at high levels by initial lymphatics, but mostly absent in LV collectors [9,10]. LECs also express GP38 (podoplanin) and PECAM-1 (CD31) that they share with fibroblastic reticular cells (FRCs) and BECs, respectively. By transporting immune cells and antigens from peripheral tissues to lymph nodes (LNs), LVs are essential for the initiation of adaptive immune responses [11–14]. FRCs, BECs and LECs express a multitude of immune mediators and growth factors implicated in affecting immune functions [15]. Moreover, these cells are specialized for their unique microenvironment [15], which might reflect a functional cell specialization depending on the organ microenvironment, as also suggested by a recent comparative study of LN-LECs, LN-BECs and diaphragm-LECs [16]. LECs modulate immune responses in various ways. By releasing sphingosine 1-phosphate (S1P), LN-LECs not only allow activated T cells to exit from LNs [17,18], but also promote naïve T cell survival and steady-state recirculation [19]. LECs exposed to T-cell derived inflammatory signals (IFN-γ and TNF) produce nitric oxide, inhibiting T cell activation and proliferation [20]. Finally, during inflammation, LECs in collecting LVs or in the skin suppress dendritic cell (DC) maturation via a Mac-1/ICAM-1 dependent mechanism [21], or through prostacyclin synthesis [22], leading to reduced T cell activation.

LECs can also function as *bona fide* antigen-presenting cells. Steady-state murine LN-LECs present endogenously expressed tissue-restricted antigens through MHC class I (MHCI) molecules to autoreactive $CD8^+$ T cells to induce their deletion, therefore contributing to peripheral T cell tolerance [23–25]. Furthermore, LN-LECs can cross-present exogenous antigens to $CD8^+$ T cells, inducing their apoptosis [26]. Whether LECs present antigens through MHC class II (MHCII) molecules remains debated. A study showed that steady-state LECs lack the antigen presentation MHCII restricted machinery [27]. On the other hand, we demonstrated that MHCII expression by LECs results from both endogenous molecules and MHCII-peptide complexes acquired from DCs. LECs can further present DC-derived complexes to $CD4^+$ T cells to induce their dysfunction [28]. Furthermore, the genetic abrogation of endogenous MHCII in LN stromal cells induces signs of autoimmunity in aging mice, with a possible role of LECs in impacting Tregs [29]. It was recently showed that expression of a self-antigen in LECs and FRCs induced conversion of $CD4^+$ T cells into Tregs, although it is possible that, in addition to a direct antigen presentation by stromal cells, LN DCs contribute to this effect by presenting antigens transferred by LECs or FRCs [30].

TA-LVs are required for the initiation of anti-tumor T cell responses, promoting tumor antigen drainage and DC migration from the tumor bed to the tumor-draining LNs (TdLNs), and the subsequent activation of tumor-specific naïve T cells [31]. However, using lymphangiogenic mouse melanoma, we have shown that LECs in TdLNs cross-present tumor antigens through MHCI molecules, and further drive the apoptosis of tumor-specific $CD8^+$ T cells [32]. Although in this model, enhanced tumor lymphangiogenesis also correlated with increased tumor-infiltrating Treg, whether and how LECs impact the Treg compartment was not investigated. More recently, it was demonstrated that the immunosuppressive molecule PD-L1 is upregulated by LECs following antigen specific interaction with $CD8^+$ T cells *in vitro* [33]. *In vivo*, compared to naïve skin LECs, TA-LECs express elevated levels of PD-L1 following exposure to IFN-γ present in the TME [33,34], and induce the deletion of tumor-infiltrating $CD8^+$ T cells, resulting in increased tumor growth and reduced survival [34]. TA-LECs seem however to be beneficial for the response of the TME to immunotherapies such as PD-1 blocking antibodies [35].

Reasoning that endogenous MHCII expression in LECs is IFN-γ inducible [28], and this cytokine being present at different levels in several tumors, we wondered whether and how LECs would function as MHCII-restricted antigen-presenting cells in the context of tumor development and impact anti-tumor immunity and tumor growth. First, we demonstrated that in tumors, LECs upregulate MHCII in response to IFN-γ produced by immune cells, as well as the MHCII-related antigen presentation machinery, and exhibit an increased ability to capture and process exogenous antigens. Using different mouse models of lymphangiogenic tumors, we provide evidence that the abrogation of MHCII in LECs results in impaired tumor growth and enhanced numbers of T cell effectors infiltrating the tumors. In the absence of MHCII expression by LECs, Tregs were altered locally in tumors, resulting in increased anti-tumor T cell immunity. Treg in tumors, but not in tumor TdLNs exhibited an impaired phenotype and reduced suppressive functions. Altogether, our study places LECs at the forefront of immunoregulatory players in the TME as tolerogenic antigen-presenting cells that inhibit anti-tumor immunity.

MATERIALS AND METHODS

Mice and treatments

Female wild type mice (Charles River), Rag2$^{-/-}$ (Charles River), OT2 [36], ProxCre^{ERT2} [37] crossed with MHCII$^{f/f}$ (MHCII$^{\Delta Prox-1}$) [29] and IFNγR2$^{f/f}$ [38], Foxp3^{RFP}RORγt^{GFP} [39], DEREG [40], were used between ages of 7–12 weeks. All mice had a pure C57BL/6 background and were bred and maintained under SPF conditions at the animal facility of Geneva Medical School and under EOPS conditions at Charles River in France. All procedures were approved and performed in accordance with the guidelines of, and with the approval of, the animal research committee of Geneva. ProxCre^{ERT2}MHCII$^{f/f}$ (MHCII$^{\Delta Prox-1}$), MHCII$^{f/f}$ control (MHCII^{WT}), ProxCre^{ERT2} IFNγR2$^{f/f}$ (IFNγR2$^{\Delta Prox-1}$) and IFNγR2$^{f/f}$ control (IFNγR2^{WT}) mice were treated intraperitoneally with tamoxifen (T5648, Sigma-Aldrich), 10 mg/mouse twice a day for 4 days. All procedures were performed two weeks after the last tamoxifen injection.

Bone marrow (BM) chimeric mice were generated as previously described [41]. Briefly, BM cells from Foxp3^{RFP}RORγt^{GFP} or DEREG were recovered from tibia and femurs of donor mice, and 5–7×10^6 cells were injected intravenously into sub-lethally irradiated recipient MHCII$^{\Delta Prox-1}$ and MHCII^{WT} mice (two consecutive doses of 500 cGy with 4 hours interval). Reconstitution in BM chimeric Foxp3^{RFP}RORγt^{GFP}→MHCII$^{\Delta Prox-1}$ and Foxp3^{RFP}RORγt^{GFP}→MHCII^{WT} mice, as well as BM chimeric DEREG→MHCII$^{\Delta Prox-1}$ and DEREG→MHCII^{WT} mice was assessed by analysing blood cells by flow cytometry after 6–8 weeks.

IFN-γ (Peprotech) was injected subcutaneously in both flanks (1μg/50μl). Anti-CD25 (clone PC-61.5.3) antibody or isotype control antibody (BioXcell) was administrated intratumorally (50 μg/mouse) in mice at day 11, 14 and 16 after tumor inoculation. DQ Ovalbumin (D-12053) (Molecular Probes) was injected intratumorally (6 μg/mouse). Diphtheria toxin (D0564–1MG-Sigma) was administrated intratumorally (0.2 μg/mouse) in mice at day 15 and 17 after tumor inoculation.

LEC/FRC in vitro culture

A mixture of FRC/LEC culture was performed as previously described [24]. In brief, LNs from 1–3 mice were dissected and digested with a freshly made enzymatic solution comprised of RPMI-1640 containing 0.8 mg/ml Dispase, 0.2 mg/ml Collagenase P, and 0.1 mg/ml DNase I (Roche). Tubes were incubated at 37°C in a water bath and gently inverted at 10-min intervals to ensure the contents were mixed. After 20 min, LNs were very gently mixed using a 1-ml pipette. Large fragments were allowed to settle before replacing the supernatant for fresh digestion mix. Supernatant containing the digested cells was added into 10 ml of cold FACS buffer (2% FCS and 5 mM EDTA in PBS). These steps were repeated every 10 min until all LNs were completely digested. Cells were washed and filtered through a 70-μm cell strainer, quantified using a hemocytometer, and plated in 6-well plates at a concentration of 1 × 10^7 cells/well. Cell culture media was MEM supplemented with 10% batch-tested, low Ig FCS, and 1% penicillin/streptomycin. Plates were washed and culture media was renewed every day to remove non-adherent cells. After 5 d, cultures primarily

contained LECs and FRCs. OVA protein, OVA AlexaFluor488 (AF488) and Ovalbumin DQ (D-12053) (Molecular Probes) (1 μg/ml) were added to the culture. The frequency of cells having captured (OVA AF488) and containing proteolytic fragments (AF488 from OVA DQ) was assessed by flow cytometry.

OT2 iTreg or non-iTregs co-cultures with *in vitro* LECs

All skin LNs (inguinal, axillary, brachial) were acquired from OT2 mice, scratched and purified using a $CD4^+$ T cell isolation kit (Miltenyi Biotec), according to manufacturer's instructions. $CD4^+$ T cells were plated in a 24 well-plate coated with Ultra-LEAF™ purified anti-mouse CD3e (145–2C11), 1mg/ml and Ultra-LEAF™ purified anti-mouse CD28 (37.51): 1mg/ml 2.5×10^5 cells/well were incubated in RPMI medium and TGF-β (3ng/ml) (Miltenyi Biotec) for 2 days and then transferred in a new plate with IL-2 (20ng/ml) (Peprotech) for 3 days. After Treg differentiation, cells were co-cultured with LECs at a ratio of 1:1 for 3 days. LEC were treated with IFN-γ (2μg/ml) and loaded with OVA_{II} peptide (5μg/ml) overnight prior to co-culture.

For OT2 $CD4^+$ T cell coculture with *in vitro* LECs: All skin LNs (inguinal, axillary, brachial) were harvested from OT2 mice, scratched and purified using a $CD4^+$ T cell isolation kit (Miltenyi Biotec), according to manufacturer's instructions. LEC were treated with IFN-γ (2μg/ml) and loaded with different doses of OVA_{II} peptide (5μg/ml, 250ng/ml and 12.5ng/ml) overnight prior to co-culture. OT2 $CD4^+$ T cells were co-cultured with LECs at a ratio of 1:1 for 7 days under Treg polarization condition (TGF-β at 3ng/ml and IL-2 at 5ng/ml).

Tumor cell lines

B16F10-OVA^+ and B16F10-OVA^+VEGF-C^{hi} melanoma cells [32] were maintained in RPMI (GIBCO Invitrogen, Grand Island, NY) supplemented with 10% heat-inactivated fetal bovine serum (FBS) (GIBCO Invitrogen), 1% penicillin-streptomycin and 0.1% of β-mercaptoethanol (GIBCO Invitrogen). MC-38 murine colon adenocarcinoma cells transduced with the lentiviral murine Vegfc cDNA (MC-38 VEGF-C^{hi}) were kindly provided by T. Petrova. Murine lung adenocarcinoma $Kras^{-/-}p53^{-/-}$ tumor cells [42,43] were kindly provided by T. Jacks' laboratory.

Tumor cell inoculation and tumor measurement

Mice were anesthetized using isoflurane or a mix of Rompun/ketamine and their backs were shaved. 0.5×10^6 B16F10-OVA^+, B16F10-OVA^+VEGF-C^{hi} or MC-38-OVA^+VEGF-C^{hi} cells were injected in 100μl of PBS subcutaneously on the back dorsolateral side of the mice. Tumor size was monitored every 1–2 days using a caliper and tumor size was calculated by length x width. 0.5×10^6 murine lung adenocarcinoma $Kras^{-/-}p53^{-/-}$ tumor cells were injected i.v. and lung tumor nodules were monitored using X-Ray Computed Tomography (Quantum GX microCT imaging system).

Cell isolation

Skin, LNs, and tumors were cut into small pieces and digested in RPMI containing 1 mg/ml collagenase IV (Worthington Biochemical Corporation), 40 μg/ml DNase I (Roche), and 2%

FBS for 30 min at 37 °C. remaining tissue was further digested with 1 mg/ml collagenase D, and 40 μg/ml DNase I (Roche) and 1% of FBS for 20 min at 37 °C. Stromal. The reaction was stopped by addition of 5 mM EDTA and 10% BSA. Samples were further disaggregated through a 70μm cell strainer and blocked with anti-CD16/32 antibody. Single-cell suspensions were further selected using CD45 microbeads and a magnetic bead column separation (Miltenyi Biotec).

OT2 $CD4^+$ T cell co-cultures with *ex vivo* LECs

All skin LNs (inguinal, axillary, brachial) were acquired from OT2 mice, scratched and purified using a $CD4^+$ T cell isolation kit (Miltenyi Biotec), according to manufacturer's instructions. Naïve $CD4^+$ T cells ($CD4^+CD25^-$) were sorted and plated with LECs sorted from TdLN and tumor, and were co-cultured for 3 days. LEC were loaded with OVA_{II} peptide (5μg/ml) overnight prior to co-culture.

Treg suppression assay

In vitro Treg suppressive assays were performed as follows: $CD4^+CD25^{hi}$ Treg cells were purified by flow cytometry from tumors and TdLNs and cultured at the different ratio with CFSE-labelled naive $CD4^+CD25^{neg}$ T cells in the presence of BM–derived dendritic cells and anti-CD3 antibodies. Labelled T-cell proliferation was assessed by flow cytometry after 3 d of co-culture.

Immunohistochemistry on tumor sections

Mouse tumors were embedded in PFA 4% for 4H, overnight in sucrose 30% and then mounted in OCT medium. 5–10-μm-thick sections were cut and fixed with paraformaldehyde 4% for 20 min. After washing and permeabilization, the sections were stained overnight at 4°C using a rabbit anti-Lyve-1 antibody (Reliatech GmbH). Secondary staining was performed using an Alexafluor546-labelled donkey anti-rabbit antibody and Alexafluor488-labelled anti-Foxp3 (150D) antibodies or eFluor660-labelled anti-Ki67 (SolA15), for 2 h at room temperature. After DAPI (Sigma- Aldrich) staining, sections were mounted with Mowiol fluorescent mounting medium (EMD). To analyze lymphatic vascularization and subtumoral distribution of Tregs in VEGF-overexpressing B16-derived melanomas ex vivo imaging of individual tumor slices was performed using an upright spinning disk confocal microscope (Axio Examiner Z1 Advanced Microscope Base, Zeiss) equipped with a confocal scanner unit CSU-X1 A1 (Yokogawa Electric Corporation). The fluorescence was detected with an electron-multiplying charge-coupled device camera (EMCCD, Evolve 512 10 MHz Back Illuminated, Photometrics) and a 10x/ 0.3 NA or a 40x/ 1.0 NA water immersion objective (W Plan Apochromat, Zeiss) upon visualization using three laser-excitation wavelengths (488 nm, 561 nm and 640 nm, LaserStack v4 Base, 3i) in combination with appropriate band-pass-emission filters (Semrock). Three-dimensional image stacks were obtained by sequential acquisition of multiple field of views (FOVs) along the z-axis using a motorized XY-stage (ProScan, Prior). SlideBook software (6.0.17, 3i) was used for image acquisition and the creation of maximum projections. The subsequent generation of montage images from contiguous positions was performed using the Fiji grid/ collection stitching plugin [44].

Human tumors were acquired from non-treated melanoma patients. Paraffin embedded blocks were deparaffinised and hydrated. Sections were stained overnight with primary antibodies, anti-podoplanin / gp38 antibody [D2–40] (ab77854), anti-FOXP3 antibody [SP97] (ab99963) or anti-CD3 antibody (ab16669), and subsequently DAPI (Sigma-Aldrich). Images were acquired with a confocal microscope (LSM 700; Carl Zeiss Inc. and SP5; Leica). Quantification was performed by calculating the LV density ($D2–40^+$, % of total area) and the amount of stained $Foxp3^+cells/mm^2$ or stained $CD3^+cells/mm^2$. A square root transformation on count data was applied to get in line with the assumption of normality for regression analysis.

Antibodies, flow cytometry and cell sorting

Anti-gp38 (8.1.1), anti-CD31 (390), anti-CD11c (N418), anti-CD44 (IM7), and anti-IAb (AF6.120.1) anti-CD45 (30F11). Anti-CD16/32 (93), anti-CD19 (6D5), anti-CD8 (53–6.7), anti-CD4 (GK1.5), anti-CD11b (M1/70), anti CD62L (MEL-14), anti-PDCA-1 (eBio927), anti-PD-1 (J43), anti-IFN-γ (XMG1.2), anti-IL-17 (eBio17B7), anti-Foxp3 (FJK-16s) anti-TCRβ (H57–597), anti-Ly6C (HK1.4), anti-Ly6G (1A8), anti-NKp45 (29A1.4), anti-Ki67 (SolA15), anti-CCR8 (SA214G2), anti-GranzymeB (GB11), anti-PD-L1 (10F.9G2), anti-Ter119 (TER-119), anti-CTLA-4 (UC10–4B9), were from eBioscience and/or Invitrogen. Anti-I-Ad/I-Ed (2G9), anti-ICOS (C398.4A), anti-CD103 (M290) mAb, were from BD.

For LNSC flow cytometry sorting, enriched CD45neg cells were stained with mAbs against CD45, gp38, and CD31.

Treg were isolated from tumors and LNs of $Foxp3^{RFP}ROR\gamma t^{GFP}\rightarrow MHCII^{\Delta Prox-1}$ and $Foxp3^{RFP}ROR\gamma t^{GFP}\rightarrow$MHCIIWT BM chimeric mice by flow cytometry cell sorting, after enrichment using a CD4 T cell depletion KIT (Miltenyi Biotec).

Intracellular cytokine stainings were carried out with the Cytofix/Cytoperm kit (BD) for IFN-γ and IL-17 staining. Foxp3 staining was performed with the eBioscience kit, according to manufacturer's instructions. For IFN-γ and IL-17 staining, LN cells were cultured in RPMI containing 10% heat-inactivated fetal bovine serum, 50 mM 2-mercaptoethanol, 100mM sodium pyruvate, and 100 μM penicillin/streptomycin at 37°C and 5% CO2. Cells were stimulated with PMA/ionomycin and Golgi stop solution (BD) for 4 h of culture before the staining.

Cells were either acquired on a Fortessa or sorted using a MoFlowAstrios (Beckman Coulter), and analysed using FlowJo (TreeStar) software.

RNA isolation and quantitative RT-PCR

Total RNA was isolated using Tri-Reagent (Ambien) from sorted cells. cDNA was synthesized using random hexamers and M-MLV reverse transcriptase (Promega).

PCRs were performed with the CFX Connect real-time PCR detection system and iQ SYBR green super mix (Bio-Rad Laboratories). The results were normalized with GAPDH or 60S ribosomal protein L32 mRNA expression and quantified with a standard curve generated with serial dilutions of a reference cDNA preparation.

H2-DMb1–2: fw TAGACGTCCCCGTAGGAAGG, rev CACAGAACGAGAGCGCCA*: I-Ab*: fw CTGTGGTGGTGCTGATGG, rev CGTTGGTGAAGTAGCACTCG*; CD74:* fw CGCCTAGACAAGCTGACCAT, rev AACGTTCTTCACAGGCCCAA*; CTLA-4:* fw GCTTCCTAGATTACCCCT TCT GC, rev CGGGCATGGTTCTGGATCA; *PD-1:* fw CGTCCCTCAGTCAAGAGGAG, rev GTCCCTAGAAGTGCCCAACA; *CCR8:* fw TTC CTC TAC TTA GGG AGA CAA ATG C, rev CAT CCA GGG TGG AAG AAT GG; *ICOS:* fw TCT AGA CTT GCA GGT GTG ACC, rev CAG GGG AAC TAG TCC ATG CG; *ZAP-70:* fw GCATGCGCAAGAAGCAGATT, rev GGGCCTCTCGCATCATCTC; *CD3:* fw ATGCGGTGGAACACTTTCTGG, rev GCACGTCAACTCTACACTGGT; *GAPDH:* fw CCCGTAGACAAAATCGTGAAG, rev AGGTCAATGAAGGGGTCGTTG; *L32:* fw GAAACTGGCGGAAACCCA, rev GGATCTGGCCCTTGAACCTT. For VEGF-C qPCR, a RT2 qPCR Primer Assay was used (Qiagen, Catalog no 330001 PPM03061F; Reference position: 449).

RNA sequencing

Library preparation, sequencing, and read mapping to the reference genome.—Flow cytometry–isolated Tregs (see above) were collected in RNAprotect Cell Reagent (Qiagen). RNA was isolated using a RNeasy Plus Micro Kit (Qiagen), and three to four replicates per condition were used. RNA integrity and quantity were assessed with a Bioanalyzer (Agilent Technologies). cDNA libraries were constructed by the Genomic platform of the University of Geneva as follows: the SMARTer Ultra Low RNA Kit from Clontech was used for the reverse transcription and cDNA amplification according to the manufacturer's specifications, starting with 1 ng of total RNA. cDNA (200 pg) was used for library preparation using the Nextera XT Kit from Illumina. Library molarity and quality were assessed with the Qubit and Tapestation using a DNA High sensitivity chip (Agilent Technologies). Pools of 10 libraries were loaded for clustering on a single read Illumina Flow cell. Reads of 50 bases were generated using the TruSeq SBS chemistry on an Illumina HiSeq 4000 sequencer. FastQ reads were mapped to the ENSEMBL reference genome (GRCm38.89) using STAR version 2.4.0j (https://github.com/alexdobin/STAR) with standard settings, except that any reads mapping to more than one location in the genome (ambiguous reads) were discarded (m . 1).

Unique gene model construction and gene coverage reporting.—A unique gene model was used to quantify reads per gene. Briefly, the model considers all annotated exons of all annotated protein coding isoforms of a gene to create a unique gene where the genomic region of all exons are considered coming from the same RNA molecule and merged together. RNA-seq analysis. All reads overlapping the exons of each unique gene model were reported using featureCounts version 1.4.6- p1 (http://bioinf.wehi.edu.au/featureCounts/). Gene expressions were reported as raw counts and in parallel normalized in reads per kilobase million (RPKM) in order to filter out genes with low expression value (1 RPKM) before calling for differentially expressed genes. Library size normalizations and differential gene expression calculations were performed using the package edgeR (http://bioconductor.org/packages/release/bioc/html/edgeR.html) designed for the R software (http://www.R-project.org/). Only genes having a significant fold change (Benjamini–Hochberg corrected P value < 0.05) were considered for the rest of the RNA-seq analysis.

Gene ontology and/or KEGG analysis.—Gene ontology (GO) term and Kyoto Encyclopedia of Genes and Genomes (KEGG) metabolic pathways enrichment were performed using homemade scripts for the R software.

Multi-Dimension Plot.—The distance between each pair of samples is the root-mean-square deviation for the top 500 most variable genes. Distances on the plot can be interpreted as leading log2 fold-change, meaning the typical (root-mean-square) log2 fold-change between the samples for the genes that distinguish those samples.

Heatmaps.—A GSEA (Gene Set Enrichment Analysis) yielded a list of upregulated pathways (pathways with FDR (False Discovery Rate) lower than 0.05 and abs(NES) (Normalized Enrichment Score) higher than 1) that was then sorted for immunological relevance: hematopoietic cell lineage, Th1,Th2, Th17 differentiation pathway, cytokine-cytokine receptor interaction, inflammatory response pathway, T-cell receptor signalling pathway, NFkB signalling pathway, cytokines and inflammatory response, Il-17 signalling pathway, type II interferon signalling, chemokine signalling, TNF signalling, Jak-Stat signalling and PD-L1 and PD-1 checkpoint pathway in cancer. Genes with a low enrichment score and a fold change lower than 0.05 were excluded. Heatmaps display expression levels in ln(1+RPKM) (Reads Per Kilobase per Million) in false colors. For heatmaps with z-score: a z-score was applied on each row, to highlight high fold changes. *GEO depository number*: GSE168609 (https://www.ncbi.nlm.nih.gov/geo/query/acc.cgi?acc=GSE168609).

Statistical analysis

Statistical significance was assessed by the two-tailed unpaired Student's t test, unpaired, non-parametric t-test and ANOVA using Prism 5.0 software (Graph- Pad Software).

RESULTS

Tumor lymphangiogenesis increases primary tumor growth

Using the B16F10-OVA^{+}VEGF-C^{hi} (B16-OVA^{+}VC^{hi}) lymphangiogenic mouse melanoma model [32], flow cytometry analysis revealed that the frequency of LECs (CD45^{neg}CD31^{+}gp38^{+}) in VEGF-C^{hi} tumors was largely increased compared to the control parental B16F10-OVA^{+} (B16-OVA^{+}) tumors (Fig. 1A), confirming previously published immunohistochemistry data on tumor sections [32] that VEGF-C produced by the tumor induces LEC expansion. In contrast, the frequency of BECs remains similar in both lymphangiogenic and non-lymphangiogenic tumors (Fig. 1A). Interestingly, VEGF-C overexpression in tumors affected the size of primary tumors, which was increased in comparison to non-lymphangiogenic control tumors (Fig. 1B). Both tumors grew similarly when transplanted into Rag2$^{-/-}$ immunodeficient mice (Supplementary Fig. S1), indicating that LECs in the TME promote immunosuppression by regulating anti-tumor adaptive immunity.

Tumoral LECs function as MHCII-restricted antigen-presenting cells

In order to determine whether LECs function as MHCII-restricted antigen-presenting cells in B16-OVA^{+}VC^{hi} tumor context, we first analysed their MHCII expression levels. Compared

to their steady-state skin LEC counterparts and LN LECs, TA-LECs expressed elevated levels of MHCII mRNA (Fig. 1C). At the protein level, LECs in tumors exhibited enhanced MHCII surface expression compared to skin LECs, and furthermore compared to TdLN and non-draining LNs (NdLN) (Fig. 1D). LECs express the IFN-γ inducible promoter IV of CIITA [28], the master regulator for MHCII expression [45]. To investigate whether IFN-γ produced in the TME promotes the upregulation of MHCII by LECs, we used ProxCre^{ERT2} mice crossed to IFNγR2$^{f/f}$ (IFNγR2$^{\Delta Prox-1}$) to abrogate IFNγR2 in LECs. MHCII expression was strongly reduced in intratumoral LECs from IFNγR2$^{\Delta Prox-1}$ compared to IFNγR2^{WT} controls (Fig. 1E). Supporting the notion that LECs in B16-OVA^{+}VC^{hi} tumors could function as MHCII-restricted antigen-presenting cells, invariant chain (CD74) mRNA was increased in tumor LECs compared to skin LECs, although expressed at lower levels compared to LN LECs (Fig. 1F). In addition, levels of H2-DM mRNA were elevated in LECs from tumors compared to skin or LNs (Fig. 1F). Therefore, tumor LECs express significant mRNA levels of the machinery implicated in MHCII-related antigen presentation. LEC proliferation has been shown to be a prerequisite for antigen acquisition [46]. When cultured *in vitro*, LECs were highly proliferative (Supplementary Fig. S2A) and, when incubated with the OVA protein coupled to Alexa Fluor 488 (OVA AF488), they proved highly competent, even superior compared to bone marrow-derived DCs (BMDC), at capturing exogenous antigens (Supplementary Fig. S2B). Most importantly, when incubated with the pH-sensitive OVA DQ, which releases fluorescent fragments upon proteolytic digestion, LECs were fluorescent after both 4h and 12h, demonstrating that *in vitro* LECs were capable of targeting exogenous antigens to late endosomal compartment (Supplementary Fig. S2B). *In vivo*, whereas LECs in normal skin are poorly proliferative, LECs in B16-OVA^{+}VC^{hi} tumors undergo an extensive proliferation (Fig. 1G, Supplementary Fig. S2C), likely mediated by elevated VEGF-C levels in the TME. TdLN LEC expansion was more modest, still significantly higher compared to NdLN LECs (Fig. 1G). Intratumoral OVA DQ injection resulted, after 4 hours, in a robust antigen capture and access to late endosomal compartments in LECs from tumors and, to a lesser extent, in LECs from TdLNs (Fig. 1H). In tumors, LEC ability to process antigens was comparable, even slightly higher, to DCs. These results show that TA-LECs capture and process exogenous antigens in lymphangiogenic tumors. We also assessed parental poorly lymphangiogenic B16-OVA^{+} tumors, comparing MHCII and PD-L1 expression, proliferation, and exogenous Ag capture and processing by LECs from B16-OVA^{+}VC^{hi} and parental B16-OVA^{+} tumors. MHCII and PD-L1 expression by LECs were not altered by the overexpression of VEGFC in tumors (Supplementary Fig. S3A). About 40% of LECs in parental B16-OVA^{+} tumors proliferated (Supplementary Fig. S3A). As expected given the lymphangiogenic functions of VEGF-C, LECs proliferated more in B16-OVA^{+}VC^{hi} compared to parental B16-OVA^{+} tumors (60% compared to 40% of proliferating LECs, respectively) (Supplementary Fig. S3A). In addition, and in agreement with the literature suggesting that proliferating LECs exhibit elevated Ag capture ability [46], LECs from both B16-OVA^{+} and B16-OVA^{+}VC^{hi} tumors were found competent at capturing and processing OVA DQ exogenous protein (Supplementary Fig. S3B). Altogether, our data indicate that LECs ability to express MHCII, proliferate and capture and process exogenous Ags in tumors is not dependent on VEGF-C overexpression.

In order to determine whether LECs demonstrate functional MHCII-restricted antigen presentation functions, we exposed cultured LECs to IFN-γ and loaded them with OVA_{II} peptide, before co-incubating them with OVA-specific $CD4^+$ induced Treg (iTregs) or non Tregs (non-iTregs) (generated in vitro from OT-2 cells). Interestingly, after 3 days of co-culture, LECs efficiently promote OT2 iTreg cell expansion and accumulation, whereas they seem to induce an abortive proliferation of non-iTreg $CD4^+$ OT2 T cells, with increased T cell death (Supplementary Fig. S3C). The ability of OVA_{II}-loaded, IFN-γ treated LECs to induce Tregs from naïve OT-2 cells under Treg-polarizing condition was dose dependent (Supplementary Fig. S3D). LECs induced the expansion and the activation of Tregs with minimal cell death, whereas non Tregs cells required higher amounts of antigen presented by LECs, were less efficiently activated, proliferated less, and died more (Supplementary Fig. S3D). To confirm this in vivo, LECs were sorted from B16-OVA^+VC^{hi} tumors or TdLNs, loaded with OVA_{II} peptide, and co-cultured with $CD4^+$ OT2 T cells. Whereas TdLNs LECs were not capable of inducing OT2 proliferation, tumor LECs promoted the proliferation and/or differentiation of $Foxp3^+$, but not $Foxp3^-$ OT2 cells (Fig. 1I). Altogether, our data demonstrated that LECs in tumors exhibit enhanced MHCII presentation machinery and are capable of capturing and directing exogenous antigens to lysosomal endocytic compartment. In addition, LECs in tumors can present the tumor model antigen OVA to antigen-specific OT2 to induce Treg proliferation. This suggests that the TME, and/or lymphangiogenic factors, promote LEC ability to function as bona fide MHCII-restricted antigen-presenting cells.

MHCII abrogation in LECs reduces tumor growth and improves tumor T cell immunity

Next, we generated mice to selectively abrogate MHCII in LECs. Prox-1-Cre^{ERT2} mice were crossed with $MHCII^{fl/fl}$ mice, referred as $MHCII^{\Delta Prox-1}$ mice, to allow the selective deletion of MHCII in LECs upon Tamoxifen (Tx) treatment. $MHCII^{fl/fl}$ mice were used as controls ($MHCII^{WT}$). The efficacy, as well as the selectivity of the deletion was tested *in vivo*, by injecting IFN-γ s.c. to induce MHCII upregulation in LECs, BECs and FRCs [29], and harvesting the draining LNs after 24h. Tx administration leads to a specific abrogation of MHCII upregulation induced by IFN-γ in LECs, but not in BECs and FRCs (Supplementary Fig. S4). B16-OVA^+VC^{hi} tumor cells were injected into Tx-treated $MHCII^{\Delta Prox-1}$ and $MHCII^{WT}$ mice, and tumoral LECs and BECs were analysed for their expression of MHCII molecules. Again, MHCII expression was abrogated only in LECs from $MHCII^{\Delta Prox-1}$ but not from $MHCII^{WT}$ mice, whereas BECs were unaffected (Fig. 2A). We also investigated whether deletion of MHCII impacted other LEC characteristics, but could not find any differences in terms of frequency, densities, nor expression of PD-L1 by LECs infiltrating tumors in $MHCII^{\Delta Prox-1}$ and $MHCII^{WT}$ mice (Supplementary Fig. S5A).

B16-OVA^+VC^{hi} tumor growth follow-up revealed a significant decrease in the size of tumors developing in LEC-restricted absence of MHCII expression, with about a two-fold reduction in $MHCII^{\Delta Prox-1}$ compared to $MHCII^{WT}$ mice at day 16 (mean tumor size at day 16, 109,4±36.2 mm^2 and 203,1±7.2 mm^2, and AUC 767,7 and 451,9, respectively) (Fig. 2B). Effector T cells analysis at day 10 in the TdLNs did not show any difference in the numbers of IFN-γ producing $CD4^+$ T cells, nor of IFN-γ producing $CD8^+$ T cells (Fig. 2C), suggesting that MHCII abrogation in LECs does not affect the priming of

anti-tumor T cells. In contrast, densities of both tumor-infiltrating IFN-γ producing $CD4^+$, and IFN-γ and Granzyme-B producing $CD8^+$ T cell effectors, were significantly increased in tumors from $MHCII^{\Delta Prox-1}$ compared to $MHCII^{WT}$ mice (Fig. 2D). Numbers of other tumor-infiltrating immune cells, such as DCs, myeloid derived suppressor cells, and natural killer cells, were not impacted by the absence of MHCII in LECs (Supplementary Fig. S5B). In contrast, neutrophils were more abundant in tumors in which LECs do not express MHCII (Supplementary Fig. S5B).

Supporting the hypothesis that MHCII expression by LEC attenuates effector T cells in tumors in less lymphangiogenic tumors, we also see a difference in tumor growth of parental B16-OVA^+ tumors in absence of MHCII expression by LECs. Although the effect is less pronounced compared to its lymphangiogenic version, B16-OVA^+ tumors were significantly smaller in $MHCII^{\Delta Prox-1}$ compared to $MHCII^{WT}$ control mice (Supplementary Fig. S6A). In addition, there is a tendency of increased effector T cell densities ($IFN\gamma^+CD8^+$ and $IFN\gamma^+CD4^+$ T cells) (Supplementary Fig. S6B) in tumors from $MHCII^{\Delta Prox-1}$ compared to $MHCII^{WT}$ control mice. Therefore, in low lymphangiogenic tumors as well, MHCII expression by LECs promotes tumor growth and attenuate intratumoral effector T cells.

We tested a second lymphangiogenic tumor mouse model which does not express the tumor model Ag OVA, the MC-38 line derived from C57BL/6 murine colon adenocarcinoma cells overexpressing VEGF-C (MC-38-VEGF-C^{hi}, referred MC-38-VC^{hi}). *In vitro* VEGF-C mRNA levels in MC-38-VC^{hi} cell cultures were increased around 10-fold compared to MC-38 parental cell line, however 10-fold less compared to B16-OVA^+VC^{hi} cells (Supplementary Fig. S7A). Accordingly, we could detect LECs in MC-38-VC^{hi} tumors, although the frequency was much lower compared to B16-OVA^+VC^{hi} tumors (Supplementary Fig. S7B). First, we compared the growth of parental MC-38 and MC-38-VC^{hi} tumors. MC-38-VC^{hi} tumors grew significantly faster compared to their non-lymphangiogenic version (Supplementary Fig. S7C). Therefore, although LECs are less numerous in MC-38-VC^{hi} compared to B16-OVA^+VC^{hi} tumors (Supplementary Fig. S7B), lymphangiogenesis promotes tumor growth in this tumor model as well. Tx treatment induced an abrogation of MHCII in tumoral LECs from MC-38-VC^{hi} tumor bearing $MHCII^{\Delta Prox-1}$ mice (Fig. 3A), and did not impact LEC frequencies, densities, or their expression of PD-L1 in tumors (Supplementary Fig. S7B). Furthermore, in MC-38-VC^{hi} tumor bearing C57BL/6 mice, LECs in tumors and TdLNs proliferate extensively and significantly more compared to ndLNs and skin LECs (Supplementary Fig. S7D). Even though LECs were less abundant compared to B16-OVA^+VC^{hi} tumors, MC-38-VC^{hi} tumors growth was also significantly reduced in $MHCII^{\Delta Prox-1}$ compared to $MHCII^{WT}$ (Fig. 3B). Effector T cell responses remained unaffected in TdLNs (Figure 3C). However, tumor-infiltrating IFN-γ^+ effector $CD4^+$ and IFN-γ^+/Granzyme-B^+ $CD8^+$ T cell densities were increased (Fig. 3D) in $MHCII^{\Delta Prox-1}$ compared to $MHCII^{WT}$ mice, recapitulating what we observed in B16-OVA^+VC^{hi} tumors. Altogether, our results demonstrate that lymphangiogenic tumor growth is impaired in mice lacking MHCII expression in LECs, and is accompanied by enhanced $CD4^+$ and $CD8^+$ T cell effector responses in tumors. Supporting these results, tumor incidence was also found reduced in $MHCII^{\Delta Prox-1}$ compared to $MHCII^{WT}$ mice injected with non-small cell lung cancer line derived from

spontaneous murine lung adenocarcinoma Kras$^{-/-}$p53$^{-/-}$ tumor cells [42,43], which induce the development of spontaneously lymphangiogenic tumor nodules in lungs (Fig. 3E-G).

Tumor LV density correlates with intratumoral Treg accumulation in both murine and human melanoma

Our data demonstrate that numbers of both CD4$^+$ and CD8$^+$ T cell effectors infiltrating the tumors were increased in MHCII$^{\Delta Prox-1}$ mice. Together with the fact that LECs promote Treg proliferation *in vitro* and *ex vivo* (Supplementary Fig. S3C and Fig.1I) we reasoned that an active mechanism of suppression by Tregs might have been lost in absence of MHCII expression by LECs. We first investigated whether Tregs localize close to LVs in tumors. Immunofluorescence analyses showed that Tregs are more abundant in LV-rich compared to LV-free areas of B16-OVA$^+$VC^{hi} tumors, and are enriched in proximity to LVs (Supplementary Fig. S8). Thick tissue sections further identified T cells (CD3$^+$) to be located proximal to LVs, and to contain a detectable fraction of Foxp3$^+$ Tregs in close proximity to LVs (Fig. 4A). Intensity quantification proved that the Foxp3$^+$ signal (green peaks) is largely nuclear (surrounded by red CD3 peaks) and overlaps with DAPI, and exists outside (upper panels) and inside (lower panels) LVs (grey peaks) (Supplementary Fig. S9). Furthermore, sections of human melanoma tumors revealed that CD3$^+$ T cell numbers were enriched in LV-rich compared to LV-free areas (Fig. 4B). Strikingly, Foxp3$^+$ Treg numbers and LV density exhibited a more pronounced positive correlation (Fig. 4C), demonstrating that Tregs are particularly enriched in LV rich areas of human melanoma.

Tumor lymphangiogenesis is associated with T cell immunosuppression

In mice, flow cytometry data showed that Foxp3$^+$CD25^{hi} Treg frequencies were increased in B16-OVA$^+$VC^{hi} tumors compared to parental B16-OVA$^+$ tumors at day 11 (Fig. 5A). Moreover, TA-LEC and tumor infiltrating Treg densities positively correlated, with a more significant association at day 10 compared to day 14 post-tumor inoculation (Fig. 5B). Expectedly, Treg and Granzyme B$^+$ effector CD8$^+$ T cell densities negatively correlated, especially at day 14 (Fig. 5C). Effector CD4$^+$ T cells and LV densities also positively correlated, but to a lesser extent compared to Tregs (Fig. 5D and 5E). In contrast, no positive association was observed between LV densities and IFN-γ or TNFα producing CD8$^+$ T cells infiltrating the tumors (Fig. 5F and 5G). Lastly, LV densities and Granzyme B$^+$ producing CD8$^+$ T cells demonstrated negative correlations, especially at day 14 (Fig. 5H). Our data indicate that TA-lymphangiogenesis promotes Treg accumulation, while it dampens effector CD8$^+$ T cell infiltration in tumors, suggesting that TA-LVs support an immunosuppressive environment by impacting Tregs.

Absence of MHCII expression by LECs alters tumor-infiltrating Treg phenotype

We hypothetized that IFN-γ produced by immune cells in tumors promotes MHCII upregulation by LECs, enhances their ability to function as MHCII-restricted antigen presenting cells and positively impact the Treg compartment. We next assessed whether Treg cells were altered when lymphangiogenic B16-OVA$^+$VC^{hi} tumors develop in mice lacking MHCII expression by LECs. Whereas they remained unaffected in TdLNs, both the frequency and the proliferation (Ki67$^+$ cells) of Foxp3$^+$CD25^{hi} Tregs were found significantly reduced in tumors from MHCII$^{\Delta Prox-1}$ compared to MHCII^{WT} mice (Fig. 6A).

In parental B16-OVA^{+} tumor bearing MHCII$^{\Delta Prox-1}$ compared to MHCII^{WT} mice, Treg frequencies tend to be decreased, although not significant, in absence of MHCII expression by LECs (Supplementary Fig. S6C). Together with the increase tendency in effector CD4^{+} and CD8^{+} T cells (Supplementary Fig. S6B), the ratio Treg/Teff seems to be disrupted enough in MHCII$^{\Delta Prox-1}$ mice to significantly reduce the growth of B16-OVA^{+} tumors compared to MHCII^{WT} mice (Supplementary Fig. S6A).

We next performed RNA sequencing on Tregs isolated from TdLNs and tumors from mice in which LECs are sufficient or not for MHCII. To properly isolate Tregs based on their specific marker Foxp3, we generated bone marrow (BM) chimeric mice. Tx treated MHCII$^{\Delta Prox-1}$ and MHCII^{WT} mice were irradiated and reconstituted with BM cells from Foxp3^{RFP}RORγt^{GFP} mice. BM chimeric Foxp3^{RFP}RORγt^{GFP}→MHCII^{WT} and Foxp3^{RFP}RORγt^{GFP}→MHCII$^{\Delta Prox-1}$ mice were injected with B16-OVA^{+}VC^{hi} tumors. At day 12, RFP^{+}Tregs were purified from tumors and TdLNs (Supplementary Fig. S10A). Two dimensional-scaling analysis revealed that Tregs from MHCII^{WT} mice clustered separately when sorted from either TdLNs or tumors (Fig. 6B), suggesting that they exhibit a distinct phenotype. Detailed analysis showed that in MHCII^{WT} mice, genes implicated in Treg suppressive functions were upregulated in tumor Tregs compared to TdLN Tregs (such as Pdcd1 known as PD-1, cd274 known as PD-L1, ctla4, IL-10, Tgfb1, Icos, IL2RA known as CD25, Tnfrsf4 known as OX40, Tnfrsf18 known as GITR). Furthermore, tumor Tregs showed a tumor-specific signature, with an upregulation of genes such as CCR8, CCR6, Il12rb1, Irf4, Il1r2, Il21r, and increased TCR signalling (such as Zap70, Cdc247, Lat, Rac2, Cd3, Lck) (Fig. 6C; Supplementary S10B). Therefore, upon migration from LNs to tumors, Tregs are exposed to a transcriptional program which is the combination of tissue adaptation, and, as described in both human and mice, of intra-tumoral signature [6,7,47]. TdLN Tregs from Foxp3^{RFP}RORγt^{GFP}→MHCII$^{\Delta Prox-1}$ and Foxp3^{RFP}RORγt^{GFP}→MHCII^{WT} mice demonstrated a similar gene expression pattern, with minor changes in the above-mentioned genes (Fig. 6C; Supplementary S10B). These observations confirm that, as suggested by comparable effector T cell responses in TdLNs in MHCII$^{\Delta Prox-1}$ and MHCII^{WT} mice (Fig. 2C), Tregs were not impacted by the loss of MHCII expression by LECs in TdLNs. In contrast, Tregs isolated from tumors of Foxp3^{RFP}RORγt^{GFP}→MHCII$^{\Delta Prox-1}$ clustered separately (Fig. 6B), and did not upregulate genes crucial for Treg suppressive function, TCR activation, and migration to the same levels compared to Tregs from Foxp3^{RFP}RORγt^{GFP}→MHCII^{WT} tumors (Figure 6C; Supplementary S10B). Interestingly, Lta and Ltb genes, that were upregulated by Tregs in tumors compared to TdLNs in control mice, were downregulated in tumor Tregs from Foxp3^{RFP}RORγt^{GFP}→MHCII$^{\Delta Prox-1}$ mice (Fig. 6C; Supplementary S10B). Q-PCR experiments on FoxP3 $^{RFP+}$ Tregs sorted from tumors and tumor-draining LNs of FoxP3 $^{RFP+}$→MHCII^{WT} and FoxP3 $^{RFP+}$→MHCII$^{\Delta Prox-1}$ BM chimeric mice confirmed that mRNA levels of PD-1, ICOS, CCR8, CTLA-4, CD3, and Zap70, were first, increased in Tregs from tumor compared to Tregs from TdLNs in control mice, and second, significantly decreased in intratumoral Tregs from FoxP3 $^{RFP+}$→MHCII$^{\Delta Prox-1}$ BM chimeras compared to intratumoral Tregs from controls (Fig. 6D). Flow cytometry experiments further confirmed that key markers implicated in Treg suppressive functions, i.e. PD-1, ICOS, CTLA-4, CD25 and CCR8, were up-regulated in tumor-infiltrating Tregs compared to TdLN

Tregs in control animals (Fig. 7A). In addition, CD103, described to be implicated in Treg suppressive functions as well, was upregulated in tumor Tregs (Fig. 7A). Apart from PD-1 which was similarly expressed by Tregs in tumor from both groups, the expression levels of these markers by Tregs remained generally lower in tumors from MHCII$^{\Delta Prox-1}$ mice compared to MHCII^{WT} mice, some being significantly reduced (ICOS, CD25 and CTLA-4), others with only a tendency (CD103, CCR8) (Fig. 7A). Altogether, our data indicate that the absence of MHCII expression by intratumoral LECs locally alters the phenotype of Tregs, which express lower levels of markers important for their tumor signature, TCR activation and suppressive function.

Tumor-infiltrating Tregs exhibit impaired suppressive functions in absence of MHCII expression by LECs

In order to assess whether, in the absence of MHCII expression by LECs in tumor bearing mice, alterations of the Treg phenotype would result in changes in tumor growth, we depleted Tregs. B16-OVA^{+}VC^{hi} tumor bearing MHCII$^{\Delta Prox-1}$ and MHCII^{WT} mice were first injected intratumorally with anti-CD25 depleting or isotype control Abs, Treg depletion efficacy being variable in tumors (Supplementary Fig. S11A). Tumor growth in mice injected with isotype control Abs recapitulated what was previously observed, with MHCII$^{\Delta Prox-1}$ mice developing smaller tumors compared to MHCII^{WT} mice (Supplementary Fig. S11B). Whereas tumors in MHCII$^{\Delta Prox-1}$ mice were not impacted by the treatment, the size of the tumors in MHCII^{WT} mice treated with anti-CD25 depleting Abs was reduced to reach MHCII$^{\Delta Prox-1}$ tumor levels (Supplementary Fig. S11B), indicating that the tumor size difference observed in non-depleted animals was due to the Treg population. This also suggests that Treg-mediated suppression was impaired in absence of MHCII expression by TA LECs. In agreement, densities of tumor-infiltrating IFN-γ producing CD4^{+} and IFN-γ and Granzyme-B producing CD8^{+} T cell effectors were restored to similar levels in MHCII$^{\Delta Prox-1}$ and MHCII^{WT} mice depleted of Tregs (Supplementary Fig. S11C). To formally confirm Treg implication, we employed a second model where BM chimeric mice were generated in order to specifically delete Tregs. BM cells from DEREG (pFoxP3 DTR-eGFP) mice were transferred into MHCII^{WT} and MHCII$^{\Delta Prox-1}$ mice, so that upon diphtheria toxin injection (DT) Tregs would be deleted (Supplementary Fig. S12). Tumor Treg depletion was more homogeneous compared to the protocol using anti-CD25 depleting Abs, with only a partial reduction (~70%) 18h after DT injection (Fig. 7B). In contrast, Treg frequencies in TdLNs were not affected (Fig. 7B). Untreated groups exhibited the tumor size difference we expected, whereas intratumoral DT injection reduced tumor growth (Fig. 7C) to a similar extend in both groups. This demonstrates that the difference in tumor growth between untreated MHCII$^{\Delta Prox-1}$ and MHCII^{WT} mice is due to Tregs. Accordingly, densities of tumor-infiltrating IFNγ producing CD4^{+} and IFNγ and Granzyme-B producing CD8^{+} T cell effectors were increased in DT-treated MHCII^{WT} injected mice compared to their non-injected counterparts (Fig. 7D). In MHCII$^{\Delta Prox-1}$ mice in contrast, Treg depletion did not impact the elevated effector T cell densities in tumors. Altogether, these experiments indicate that differences in effector T cell responses observed in non-depleted Treg MHCII$^{\Delta Prox-1}$ and MHCII^{WT} animals were a consequence of impaired Treg suppressive functions and not due to a direct effect on effector CD4^{+} T cells.

To finally assess whether Treg suppressive functions were intrinsically altered in tumors in absence of MHCII expression by LECs, we performed an *ex vivo* Treg suppressive assay. Tregs were isolated ($CD4^+CD25^{hi}$) (Fig. 7E) from tumors and TdLNs of $MHCII^{\Delta Prox-1}$ and $MHCII^{WT}$ mice, and cultured at different ratios with CFSE-labelled naïve $CD4^+$ T cells in presence of anti-CD3 antibodies. Tregs from TdLNs in $MHCII^{\Delta Prox-1}$ and $MHCII^{WT}$ mice exhibited similar ability to supress naïve T cell proliferation (Fig. 7E), further confirming that the loss of MHCII by LECs in LNs does not impact the Treg population and does not alter their immunosuppressive functions. Tregs from $MHCII^{WT}$ tumors, however, were much more potent at suppressing T cell proliferation compared to LN Tregs (Fig. 7E). Importantly, Tregs from tumors in $MHCII^{\Delta Prox-1}$ mice were much less efficient at inhibiting CFSE-labelled T cell proliferation compared to Tregs from $MHCII^{WT}$ tumors (Fig. 7E), firmly demonstrating that whereas the function of Tregs is not affected in LNs of $MHCII^{\Delta Prox-1}$ mice, MHCII expression by LECs is required locally in tumors for Tregs to fully exhibit suppressive functions.

DISCUSSION

LVs developing in the intra-tumoral and peri-tumoral zone have been recently shown to influence tumor growth in many different ways. First, circulating VEGF-C levels [48], as well as lymphangiogenesis at tumor distal sites [49,50] have been correlated with metastasis and bad prognosis. In addition, LECs lining the LVs impact primary tumor growth by modulating anti-tumor immunity. LECs interact with DCs to promote their migration from tumors to TdLNs, and are therefore essential in the initiation of tumor-specific T cell responses [51]. However, we have shown in lymphangiogenic mouse melanoma that, VEGF-C exposed LECs favour immunosuppression, and LECs in TdLNs cross-present tumor antigens through MHCI molecules to induce tumor-specific $CD8^+$ T cell dysfunction [26,32]. In agreement, our present results show that the size of lymphangiogenic B16-OVA^+VC^{hi} tumors was increased compared to parental B16-OVA^+ tumors. It has been shown that, by upregulating PD-L1, intratumoral LECs promote tumor-specific T cell deletion in several mouse models of tumors [34]. However, a recent study suggests that adoptive transfer therapies, anti-tumor vaccines, or immune checkpoint inhibitors could revert TA LEC immunosuppressive functions and be beneficial for immunotherapies [35].

LECs have also been demonstrated to play a critical role in the maintenance of peripheral self-reactive T cell tolerance, acting as a brake against autoimmune attacks. Indeed, they endogenously express peripheral tissue-restricted antigens and present them through MHCI molecules to induce $CD8^+$ T cell deletional tolerance [23,25,27,52]. Although LEC expression levels of MHCII are low at steady-state [28], our recent study suggests that $MHCII^+$ LECs might function as a brake to prevent autoimmunity in elderly mice by promoting Treg suppressive functions [29]. However, whether LECs shape $CD4^+$ T cell responses as MHCII-restricted antigen presenting cells, in particular during tumor development was surprisingly not investigated before.

Using lymphangiogenic versions of mouse melanoma (B16-OVA^+VC^{hi}) and colon carcinoma (MC38-VC^{hi}), we have found enhanced MHCII expression levels by intratumoral LECs compared to skin-LECs or LN-LECs. In mice, MHCII expression by LECs is

under the control of the promoter IV (pIV) of CIITA, the master regulator for MHCII expression [28], which is inducible by IFN-γ [45]. Accordingly, using mice in which IFNγR has been genetically abrogated in LECs, we further show that intratumoral LECs up-regulate MHCII in tumors in response to IFN-γ. Not only MHCII molecules, but also H2-DM and CD74 were up-regulated by LECs in tumors, supporting the ability of these cells to present antigens through MHCII. In agreement with previous observations showing that LEC proliferation is a prerequisite for their capacity to capture antigens [46], LECs in tumors, which are highly proliferative, exhibit an enhanced ability to capture exogenous antigens, and to process internalized antigens. LECs were previously shown to be incompetent in processing and presenting peptides through MHCII in a context of vaccination [46]. Discrepancies could be explained by an extensive proliferation of LECs in tumors, compared to relatively lower frequencies (<20%) in LNs following vaccination [46]. Therefore, the amount of antigen acquired by LECs in tumors might be increased compared to the vaccination setting.

Lastly, we show that LECs isolated from tumors and antigen-loaded promote antigen-specific Treg proliferation. Altogether, our data suggest that intratumoral LECs can act as bona fide MHCII-restricted antigen presenting cells. Lymphangiogenic tumor growth was found significantly dampened in mice in which MHCII has been abrogated in LECs, supporting a pro-tumorigenic role for $MHCII^+$ LECs. The fact that MHCII molecules are up-regulated by LECs in tumors, and not so much in TdLNs reflects either different levels of LEC sensitivity to IFN-γ, or different ranges of IFN-γ concentrations, in the two different organs. In both cases, this supports the hypothesis that LECs will function as MHCII-restricted antigen-presenting cells by acting locally in tumors. Accordingly, anti-tumor T cell effector responses were significantly enhanced in tumors, but not affected in TdLNs, of mice in which MHCII was abrogated in LECs. We could recapitulate key results in poorly lymphangiogenic parental B16-OVA^+ tumors: tumoral LECs express MHCII, capture and process exogenous Ags, suggesting that their MHCII-restricted antigen-presenting ability is not dependent on VEGF-C overexpression. Impact of MHCII abrogation in LECs on anti-tumor T cell responses is however less pronounced in B16-OVA^+ compared to B16-OVA^+VC^{hi} tumors, with only tendencies in increased effector T cell densities and decreased Treg frequencies, with nevertheless a significant reduction in tumor size.

Our results further indicate that differences in tumor-specific effector T cell responses in $MHCII^{\Delta Prox-1}$ and $MHCII^{WT}$ mice were due to alterations of the intratumoral Treg population. First, in both murine and human melanoma, LV densities positively correlated with the number of Tregs infiltrating the tumors. Second, both Treg frequencies and proliferation were altered in tumors on $MHCII^{\Delta Prox-1}$ mice. Lastly, intratumoral Treg depletion abolished the differences in tumor growth between $MHCII^{\Delta Prox-1}$ and $MHCII^{WT}$ mice. In addition, $CD4^+$ and $CD8^+$ T effector densities in tumors from Treg-depleted $MHCII^{WT}$ mice increased to reach levels comparable to $MHCII^{\Delta Prox-1}$ mice. Interestingly, intratumoral Treg depletion in $MHCII^{\Delta Prox-1}$ mice did not affect effector T cell densities, suggesting that Tregs were already dysfunctional in absence of MHCII expression in LECs. RNA-seq data demonstrated that Treg transcriptomics were profoundly affected in tumors, but not in TdLNs, by the loss of MHCII in LECs. The tumor-specific Treg gene signature (including up-regulation of CCR8, IL12rb1, Il1r2, and Il21r), which is

conserved across species and tumor types [53], was upregulated in MHCII^{WT} mice by Treg in tumors compared to tumor dLNs. However, this signature, together with genes important in Treg adaptation and differentiation (Irf4, Irf2, CCR8) [7,54,55], and TCR signalling (such as Zap70, CD3, LcK) were lost in tumors from MHCII$^{\Delta Prox-1}$ mice. Genes important for Treg suppressive functions (ICOS, CD25, CTLA-4, PD-1) were down-regulated at mRNA levels by Tregs in tumors from MHCII$^{\Delta Prox-1}$ mice, and confirmed at surface protein levels, except for PD-1. PD-1 expression has been described to undergo post-transcriptional regulatory pathway [56], which likely explains why we observed differences between mRNA and protein expression levels. ICOS, CD25, CTLA-4, and CD103 protein expression, when taken individually, were significantly but not dramatically reduced in tumors from MHCII$^{\Delta Prox-1}$ compared to MHCII^{WT} mice. We hypothesize that the lack of MHCII expression by LECs in tumors induces a broad-spectrum of changes in Treg phenotype. Therefore, it is likely that impairments of Treg functions observed in knockout animals do not result from changes in one or the other marker, but more from a global alteration of the Treg phenotype. Altogether, we show that absence of MHCII in tumor LECs results in altered TCR signalling in Tregs, which is likely due to impaired Ag presentation by LECs, and consequently a global alteration of the Treg suppressive phenotype.

With respect to the mechanisms explaining why MHCII^{+} LECs in tumors would selectively alter Tregs and not other CD4^{+} T cell populations, two scenarios can be envisioned. Either MHCII-mediated antigen presentation by LECs in tumors is necessary to maintain a tumor-specific gene signature in already differentiated Tregs, or some naïve CD4^{+} T cells, which can be found and locally primed in tumors [57,58], differentiate into Tregs upon LEC encounter. The fact that PD-1 expression by Tregs is not affected by the loss of MHCII in LECs at protein level might support the first hypothesis, that LECs, which express higher levels of PDL-1 in the TME, preferentially establish antigen-specific interactions with already committed/activated PD-1^{hi} Tregs. Alternatively, the cross-talk between Tregs and LVs could be promoted through LTα1β2-Ltβ R pathway, which has been recently shown to promote Treg-LV interactions and suppressive functions of Tregs [59]. Accordingly, Lta and Ltb genes were upregulated by tumor Tregs compared to LNs in RNAseq results. Whatever the mechanism implicated, in contrast to LNs in which Treg suppressor activity was not altered by the loss of MHCII in LECs, Tregs isolated from MHCII$^{\Delta Prox-1}$ tumors exhibited an impaired ability to suppress the proliferation of naïve T cells ex vivo compared to Tregs from MHCII^{WT} tumors. Tregs from tumors in which LECs lack MHCII molecules actually exert suppressive functions as low as LN Tregs, demonstrating that MHCII expression by LECs is required for intratumoral Tregs to exert fully their competent suppressive functions.

B cells, macrophages/monocytes, NK, and DCs infiltrating tumors did not seem impacted by the loss of MHCII expression by LECs, although we did not precisely characterize their activation state. In contrast, neutrophil numbers were found elevated in MHCII$^{\Delta Prox-1}$ tumors. This could be explained by the alteration of the Treg compartment, since it has been described that Tregs would limit neutrophils responses in skin [60]. Further work will decipher whether not only the numbers, but also the phenotype of tumor-infiltrating neutrophils, has been altered following MHCII abrogation in LECs, and determine whether it is a consequence of Treg alterations.

Altogether, our study broadens the scope of LECs acting as immunomodulatory antigen-presenting cells during tumor development. We show that, in addition to scavenging tumor antigens and directing them to the MHCI cross-presentation pathway, tumor associated LECs target antigens to the MHCII-presentation machinery. In both cases, antigen-presenting LECs promote immunosuppression. *i)* by inducing the deletion of effector $CD8^+$ T cells through PD-L1 upregulation, or *ii)* by favouring the suppressive functions of Tregs through MHCII upregulation. Together with PD-L1[34], MHCII are up-regulated at LEC surface in the presence of IFN-γ.

Therefore, it is tempting to speculate that both PD-L1- and MHCII-mediated LEC immunosuppression will be enhanced in IFN-γ rich immunogenic tumors, a way for lymphangiogenic tumors to hijack tumor immunity.

Supplementary Material

Refer to Web version on PubMed Central for supplementary material.

ACKNOWLEDGEMENTS

The authors thank JP Aubry-Lachainaye, C Gameiro and G Schneiter for excellent assistance in flow cytometry. We also thank S Lemeille for RNAseq data analysis, T Petrova for valuable discussions and for providing MC-38 VEGF-C^{hi}, D Pejoski and A Marti Lindez for valuable discussions and/or technical help. This work was supported by the Leenaards Foundation to SH and MS, the Swiss Cancer Research foundation (KFS-3950-08-2016-R) to SH, and the Swiss National Science Foundation (310030_16654, 310030_185255) to SH.

REFERENCES

1. Motz GT, Coukos G: Deciphering and reversing tumor immune suppression. Immunity 2013, 39:61–73. [PubMed: 23890064]
2. Zitvogel L, Tesniere A, Kroemer G: Cancer despite immunosurveillance: immunoselection and immunosubversion. Nat Rev Immunol 2006, 6:715–727. [PubMed: 16977338]
3. Sakaguchi S, Yamaguchi T, Nomura T, Ono M: Regulatory T cells and immune tolerance. Cell 2008, 133:775–787. [PubMed: 18510923]
4. Fridman WH, Pages F, Sautes-Fridman C, Galon J: The immune contexture in human tumours: impact on clinical outcome. Nature reviews. Cancer 2012, 12:298–306. [PubMed: 22419253]
5. Nishikawa H, Sakaguchi S: Regulatory T cells in tumor immunity. Int J Cancer 2010, 127:759–767. [PubMed: 20518016]
6. De Simone M, Arrigoni A, Rossetti G, Gruarin P, Ranzani V, Politano C, Bonnal RJP, Provasi E, Sarnicola ML, Panzeri I, et al. : Transcriptional Landscape of Human Tissue Lymphocytes Unveils Uniqueness of Tumor-Infiltrating T Regulatory Cells. Immunity 2016, 45:1135–1147. [PubMed: 27851914]
7. Plitas G, Konopacki C, Wu K, Bos PD, Morrow M, Putintseva EV, Chudakov DM, Rudensky AY: Regulatory T Cells Exhibit Distinct Features in Human Breast Cancer. Immunity 2016, 45:1122–1134. [PubMed: 27851913]
8. Stacker SA, Williams SP, Karnezis T, Shayan R, Fox SB, Achen MG: Lymphangiogenesis and lymphatic vessel remodelling in cancer. Nature reviews. Cancer 2014, 14:159–172. [PubMed: 24561443]
9. Johnson NC, Dillard ME, Baluk P, McDonald DM, Harvey NL, Frase SL, Oliver G: Lymphatic endothelial cell identity is reversible and its maintenance requires Prox1 activity. Genes & development 2008, 22:3282–3291. [PubMed: 19056883]
10. Alitalo K, Tammela T, Petrova TV: Lymphangiogenesis in development and human disease. Nature 2005, 438:946–953. [PubMed: 16355212]

11. Olszewski WL: The innate reaction of the human skin lymphatic system to foreign and self-antigens. Lymphat Res Biol 2005, 3:50–57. [PubMed: 16000053]
12. Pugh CW, MacPherson GG, Steer HW: Characterization of nonlymphoid cells derived from rat peripheral lymph. J Exp Med 1983, 157:1758–1779. [PubMed: 6854208]
13. Mackay CR, Marston WL, Dudler L: Naive and memory T cells show distinct pathways of lymphocyte recirculation. J Exp Med 1990, 171:801–817. [PubMed: 2307933]
14. Randolph GJ, Angeli V, Swartz MA: Dendritic-cell trafficking to lymph nodes through lymphatic vessels. Nat Rev Immunol 2005, 5:617–628. [PubMed: 16056255]
15. Malhotra D, Fletcher AL, Astarita J, Lukacs-Kornek V, Tayalia P, Gonzalez SF, Elpek KG, Chang SK, Knoblich K, Hemler ME, et al. : Transcriptional profiling of stroma from inflamed and resting lymph nodes defines immunological hallmarks. Nature immunology 2012, 13:499–510. [PubMed: 22466668]
16. Berendam SJ, Koeppel AF, Godfrey NR, Rouhani SJ, Woods AN, Rodriguez AB, Peske JD, Cummings KL, Turner SD, Engelhard VH: Comparative Transcriptomic Analysis Identifies a Range of Immunologically Related Functional Elaborations of Lymph Node Associated Lymphatic and Blood Endothelial Cells. Front Immunol 2019, 10:816. [PubMed: 31057546]
17. Grigorova IL, Schwab SR, Phan TG, Pham TH, Okada T, Cyster JG: Cortical sinus probing, S1P1-dependent entry and flow-based capture of egressing T cells. Nature immunology 2009, 10:58–65. [PubMed: 19060900]
18. Pham TH, Baluk P, Xu Y, Grigorova I, Bankovich AJ, Pappu R, Coughlin SR, McDonald DM, Schwab SR, Cyster JG: Lymphatic endothelial cell sphingosine kinase activity is required for lymphocyte egress and lymphatic patterning. The Journal of experimental medicine 2010, 207:17–27. [PubMed: 20026661]
19. Mendoza A, Fang V, Chen C, Serasinghe M, Verma A, Muller J, Chaluvadi VS, Dustin ML, Hla T, Elemento O, et al. : Lymphatic endothelial S1P promotes mitochondrial function and survival in naive T cells. Nature 2017, 546:158–161. [PubMed: 28538737]
20. Lukacs-Kornek V, Malhotra D, Fletcher AL, Acton SE, Elpek KG, Tayalia P, Collier AR, Turley SJ: Regulated release of nitric oxide by nonhematopoietic stroma controls expansion of the activated T cell pool in lymph nodes. Nature immunology 2011, 12:1096–1104. [PubMed: 21926986]
21. Podgrabinska S, Kamalu O, Mayer L, Shimaoka M, Snoeck H, Randolph GJ, Skobe M: Inflamed lymphatic endothelium suppresses dendritic cell maturation and function via Mac-1/ICAM-1-dependent mechanism. Journal of immunology 2009, 183:1767–1779.
22. Christiansen AJ, Dieterich LC, Ohs I, Bachmann SB, Bianchi R, Proulx ST, Hollmen M, Aebischer D, Detmar M: Lymphatic endothelial cells attenuate inflammation via suppression of dendritic cell maturation. Oncotarget 2016, 7:39421–39435. [PubMed: 27270646]
23. Cohen JN, Guidi CJ, Tewalt EF, Qiao H, Rouhani SJ, Ruddell A, Farr AG, Tung KS, Engelhard VH: Lymph node-resident lymphatic endothelial cells mediate peripheral tolerance via Aire-independent direct antigen presentation. The Journal of experimental medicine 2010, 207:681–688. [PubMed: 20308365]
24. Fletcher AL, Lukacs-Kornek V, Reynoso ED, Pinner SE, Bellemare-Pelletier A, Curry MS, Collier AR, Boyd RL, Turley SJ: Lymph node fibroblastic reticular cells directly present peripheral tissue antigen under steady-state and inflammatory conditions. The Journal of experimental medicine 2010, 207:689–697. [PubMed: 20308362]
25. Tewalt EF, Cohen JN, Rouhani SJ, Guidi CJ, Qiao H, Fahl SP, Conaway MR, Bender TP, Tung KS, Vella AT, et al. : Lymphatic endothelial cells induce tolerance via PD-L1 and lack of costimulation leading to high-level PD-1 expression on CD8 T cells. Blood 2012, 120:4772–4782. [PubMed: 22993390]
26. Hirosue S, Vokali E, Raghavan VR, Rincon-Restrepo M, Lund AW, Corthesy-Henrioud P, Capotosti F, Halin Winter C, Hugues S, Swartz MA: Steady-state antigen scavenging, cross-presentation, and CD8+ T cell priming: a new role for lymphatic endothelial cells. Journal of immunology 2014, 192:5002–5011.

27. Rouhani SJ, Eccles JD, Riccardi P, Peske JD, Tewalt EF, Cohen JN, Liblau R, Makinen T, Engelhard VH: Roles of lymphatic endothelial cells expressing peripheral tissue antigens in CD4 T-cell tolerance induction. Nature communications 2015, 6:6771.
28. Dubrot J, Duraes FV, Potin L, Capotosti F, Brighouse D, Suter T, LeibundGut-Landmann S, Garbi N, Reith W, Swartz MA, et al. : Lymph node stromal cells acquire peptide-MHCII complexes from dendritic cells and induce antigen-specific CD4(+) T cell tolerance. The Journal of experimental medicine 2014, 211:1153–1166. [PubMed: 24842370]
29. Dubrot J, Duraes FV, Harle G, Schlaeppi A, Brighouse D, Madelon N, Gopfert C, Stokar-Regenscheit N, Acha-Orbea H, Reith W, et al. : Absence of MHC-II expression by lymph node stromal cells results in autoimmunity. Life Sci Alliance 2018, 1:e201800164.
30. Nadafi R, Gago de Graca C, Keuning ED, Koning JJ, de Kivit S, Konijn T, Henri S, Borst J, Reijmers RM, van Baarsen LGM, et al. : Lymph Node Stromal Cells Generate Antigen-Specific Regulatory T Cells and Control Autoreactive T and B Cell Responses. Cell Rep 2020, 30:4110–4123 e4114. [PubMed: 32209472]
31. Swartz MA, Lund AW: Lymphatic and interstitial flow in the tumour microenvironment: linking mechanobiology with immunity. Nature reviews. Cancer 2012, 12:210–219. [PubMed: 22362216]
32. Lund AW, Duraes FV, Hirosue S, Raghavan VR, Nembrini C, Thomas SN, Issa A, Hugues S, Swartz MA: VEGF-C promotes immune tolerance in B16 melanomas and cross-presentation of tumor antigen by lymph node lymphatics. Cell reports 2012, 1:191–199. [PubMed: 22832193]
33. Dieterich LC, Ikenberg K, Cetintas T, Kapaklikaya K, Hutmacher C, Detmar M: Tumor-Associated Lymphatic Vessels Upregulate PDL1 to Inhibit T-Cell Activation. Front Immunol 2017, 8:66. [PubMed: 28217128]
34. Lane RS, Femel J, Breazeale AP, Loo CP, Thibault G, Kaempf A, Mori M, Tsujikawa T, Chang YH, Lund AW: IFNgamma-activated dermal lymphatic vessels inhibit cytotoxic T cells in melanoma and inflamed skin. J Exp Med 2018, 215:3057–3074. [PubMed: 30381467]
35. Fankhauser M, Broggi MAS, Potin L, Bordry N, Jeanbart L, Lund AW, Da Costa E, Hauert S, Rincon-Restrepo M, Tremblay C, et al. : Tumor lymphangiogenesis promotes T cell infiltration and potentiates immunotherapy in melanoma. Sci Transl Med 2017, 9.
36. Barnden MJ, Allison J, Heath WR, Carbone FR: Defective TCR expression in transgenic mice constructed using cDNA-based alpha- and beta-chain genes under the control of heterologous regulatory elements. Immunol Cell Biol 1998, 76:34–40. [PubMed: 9553774]
37. Bazigou E, Lyons OT, Smith A, Venn GE, Cope C, Brown NA, Makinen T: Genes regulating lymphangiogenesis control venous valve formation and maintenance in mice. J Clin Invest 2011, 121:2984–2992. [PubMed: 21765212]
38. Lee HM, Fleige A, Forman R, Cho S, Khan AA, Lin LL, Nguyen DT, O'Hara-Hall A, Yin Z, Hunter CA, et al. : IFNgamma signaling endows DCs with the capacity to control type I inflammation during parasitic infection through promoting T-bet+ regulatory T cells. PLoS Pathog 2015, 11:e1004635.
39. Yang BH, Hagemann S, Mamareli P, Lauer U, Hoffmann U, Beckstette M, Fohse L, Prinz I, Pezoldt J, Suerbaum S, et al. : Foxp3(+) T cells expressing RORgammat represent a stable regulatory T-cell effector lineage with enhanced suppressive capacity during intestinal inflammation. Mucosal Immunol 2016, 9:444–457. [PubMed: 26307665]
40. Lahl K, Loddenkemper C, Drouin C, Freyer J, Arnason J, Eberl G, Hamann A, Wagner H, Huehn J, Sparwasser T: Selective depletion of Foxp3+ regulatory T cells induces a scurfy-like disease. J Exp Med 2007, 204:57–63. [PubMed: 17200412]
41. Guery L, Dubrot J, Lippens C, Brighouse D, Malinge P, Irla M, Pot C, Reith W, Waldburger JM, Hugues S: Ag-presenting CpG-activated pDCs prime Th17 cells that induce tumor regression. Cancer Res 2014, 74:6430–6440. [PubMed: 25252912]
42. Choi I, Lee S, Hong YK: The new era of the lymphatic system: no longer secondary to the blood vascular system. Cold Spring Harbor perspectives in medicine 2012, 2:a006445.
43. DuPage M, Dooley AL, Jacks T: Conditional mouse lung cancer models using adenoviral or lentiviral delivery of Cre recombinase. Nat Protoc 2009, 4:1064–1072. [PubMed: 19561589]
44. Preibisch S, Saalfeld S, Tomancak P: Globally optimal stitching of tiled 3D microscopic image acquisitions. Bioinformatics 2009, 25:1463–1465. [PubMed: 19346324]

45. Reith W, LeibundGut-Landmann S, Waldburger JM: Regulation of MHC class II gene expression by the class II transactivator. Nature reviews. Immunology 2005, 5:793–806.
46. Tamburini BA, Burchill MA, Kedl RM: Antigen capture and archiving by lymphatic endothelial cells following vaccination or viral infection. Nature communications 2014, 5:3989.
47. Miragaia RJ, Gomes T, Chomka A, Jardine L, Riedel A, Hegazy AN, Whibley N, Tucci A, Chen X, Lindeman I, et al. : Single-Cell Transcriptomics of Regulatory T Cells Reveals Trajectories of Tissue Adaptation. Immunity 2019, 50:493–504 e497. [PubMed: 30737144]
48. Tammela T, Alitalo K: Lymphangiogenesis: Molecular mechanisms and future promise. Cell 2010, 140:460–476. [PubMed: 20178740]
49. Ma Q, Dieterich LC, Detmar M: Multiple roles of lymphatic vessels in tumor progression. Curr Opin Immunol 2018, 53:7–12. [PubMed: 29605736]
50. Ma Q, Dieterich LC, Ikenberg K, Bachmann SB, Mangana J, Proulx ST, Amann VC, Levesque MP, Dummer R, Baluk P, et al. : Unexpected contribution of lymphatic vessels to promotion of distant metastatic tumor spread. Sci Adv 2018, 4:eaat4758.
51. Lund AW, Wagner M, Fankhauser M, Steinskog ES, Broggi MA, Spranger S, Gajewski TF, Alitalo K, Eikesdal HP, Wiig H, et al. : Lymphatic vessels regulate immune microenvironments in human and murine melanoma. J Clin Invest 2016, 126:3389–3402. [PubMed: 27525437]
52. Cohen JN, Tewalt EF, Rouhani SJ, Buonomo EL, Bruce AN, Xu X, Bekiranov S, Fu YX, Engelhard VH: Tolerogenic properties of lymphatic endothelial cells are controlled by the lymph node microenvironment. PloS one 2014, 9:e87740.
53. Magnuson AM, Kiner E, Ergun A, Park JS, Asinovski N, Ortiz-Lopez A, Kilcoyne A, Paoluzzi-Tomada E, Weissleder R, Mathis D, et al. : Identification and validation of a tumor-infiltrating Treg transcriptional signature conserved across species and tumor types. Proc Natl Acad Sci U S A 2018, 115:E10672-E10681.
54. Chaudhry A, Rudensky AY: Control of inflammation by integration of environmental cues by regulatory T cells. J Clin Invest 2013, 123:939–944. [PubMed: 23454755]
55. Cretney E, Kallies A, Nutt SL: Differentiation and function of Foxp3(+) effector regulatory T cells. Trends Immunol 2013, 34:74–80. [PubMed: 23219401]
56. Franchini DM, Lanvin O, Tosolini M, Patras de Campaigno E, Cammas A, Pericart S, Scarlata CM, Lebras M, Rossi C, Ligat L, et al. : Microtubule-Driven Stress Granule Dynamics Regulate Inhibitory Immune Checkpoint Expression in T Cells. Cell Rep 2019, 26:94–107 e107. [PubMed: 30605689]
57. Peske JD, Thompson ED, Gemta L, Baylis RA, Fu YX, Engelhard VH: Effector lymphocyte-induced lymph node-like vasculature enables naive T-cell entry into tumours and enhanced anti-tumour immunity. Nat Commun 2015, 6:7114. [PubMed: 25968334]
58. Thompson ED, Enriquez HL, Fu YX, Engelhard VH: Tumor masses support naive T cell infiltration, activation, and differentiation into effectors. The Journal of experimental medicine 2010, 207:1791–1804. [PubMed: 20660615]
59. Piao W, Xiong Y, Li L, Saxena V, Smith KD, Hippen KL, Paluskievicz C, Willsonshirkey M, Blazar BR, Abdi R, et al. : Regulatory T Cells Condition Lymphatic Endothelia for Enhanced Transendothelial Migration. Cell Rep 2020, 30:1052–1062 e1055. [PubMed: 31995749]
60. Richards H, Williams A, Jones E, Hindley J, Godkin A, Simon AK, Gallimore A: Novel role of regulatory T cells in limiting early neutrophil responses in skin. Immunology 2010, 131:583–592. [PubMed: 20722759]

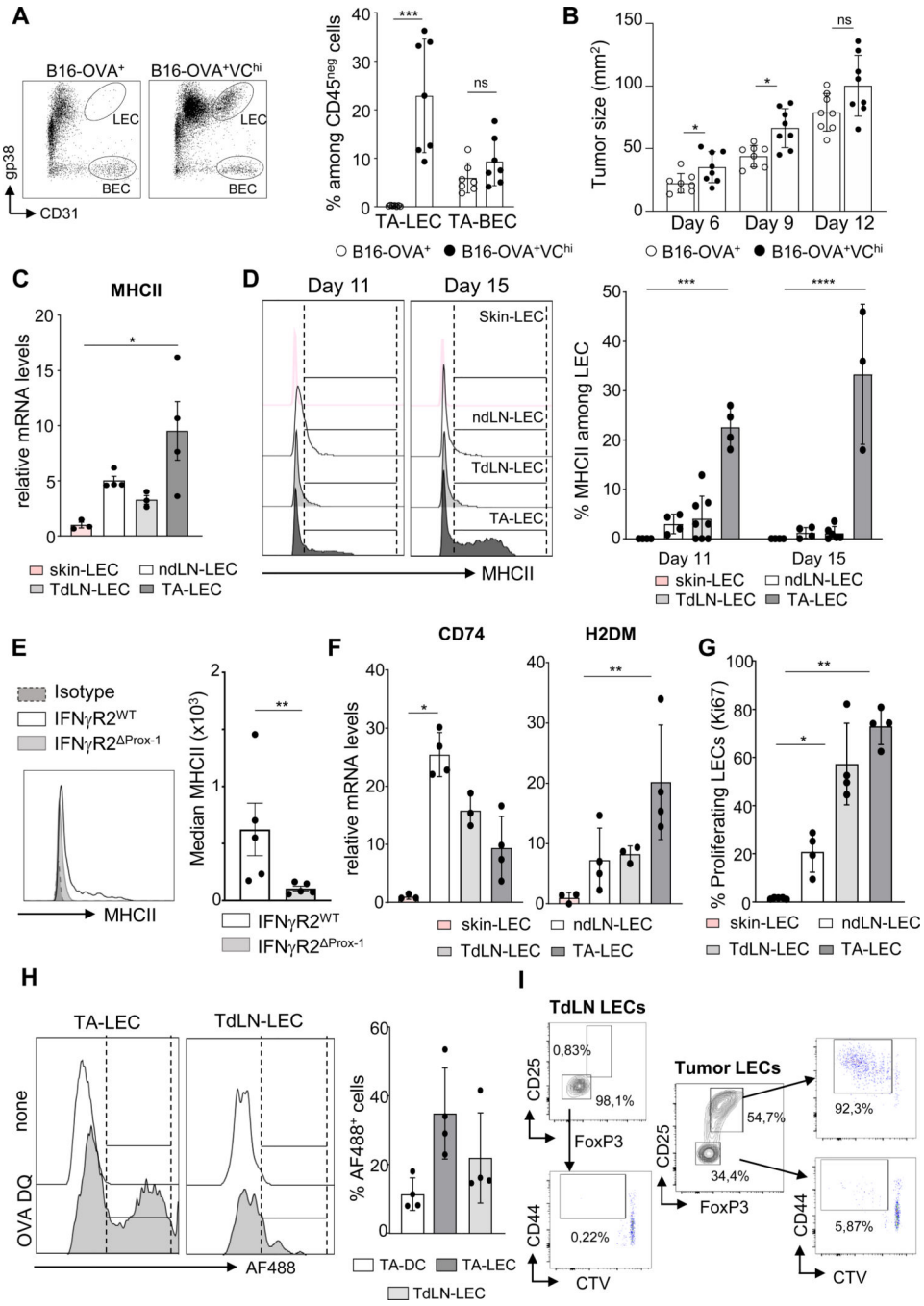

Figure 1. Lymphangiogenic tumors exhibit increased tumor growth and indicate that LECs are well equipped for MHCII-restricted antigen-presentation.

(A-B) C57BL/6 mice were injected with B16-OVA^{+} and B16-OVA^{+}VC^{hi} tumor cells. (A) Gating strategy FACS dot plot, and frequencies of lymphatic endothelial cells (LEC) and blood endothelial cells (BEC) (gated on CD45^{-} cells) (day 10). Histograms provide LEC and BEC frequencies in tumors. (B) Tumors were measured at indicated time points. Data are representative of 2 experiments with 6–7 mice per group. **(C-D)** C57BL/6 mice were injected with B16-OVA^{+}VC^{hi} tumor cells. (C) mRNA expression levels of MHCII

was measured in LECs sorted from indicated organs at day 11, levels were normalised to skin-LEC values and housekeeping genes. (D) FACS histograms showing MHCII expression levels by LECs in indicated organs at days 11 and 15 (left), and quantitative histograms (right). Data are representative of 2 experiments with 3–7 mice per group. **(E)** IFNγR2$^{\Delta Prox-1}$ and IFNγR2^{WT} mice were injected with B16-OVA^{+}VC^{hi} tumor cells and MHCII expression by LECs was analysed by FACS at day 11 in tumors. Data are representative of 2 experiments with 5 mice / group each. **(F-I)** C57BL/6 mice were injected with B16-OVA^{+}VC^{hi} tumor cells. (F) mRNA expression levels of indicated genes was measured in LECs sorted from indicated organs at day 11. (G) LEC proliferation (frequency of Ki67^{+} cells) was assessed by flow cytometry at day 11 in indicated organs. Data are representative of 3 experiments with 3–5 mice / group each. (H) DQ OVA protein was injected intratumorally at day 11. The frequency of LECs (CD45^{neg}CD31^{+}gp38^{+}) and dendritic cells (DC) containing proteolytic fragments (AF488^{+}) in tumors (TA) and TdLNs, was assessed after 4h by flow cytometry and quantified. Data are representative of 2 independent experiments with 3–4 mice / group each. (I) LECs were sorted from TdLN and tumor and co-cultured with CTV labelled CD4^{+} OTII cells for 3 days. Gating strategy on FoxP3^{+} T cells and their proliferation. Data are representative of 2 independent experiments (12 mice pooled). **(A,B)** unpaired, non-parametric t-test, **(D)** 2-way Anova **, (C,F,G)** one -way Anova. Error bars represent mean ± SD. *p <0.05; **p < 0.01; ***p < 0.001.

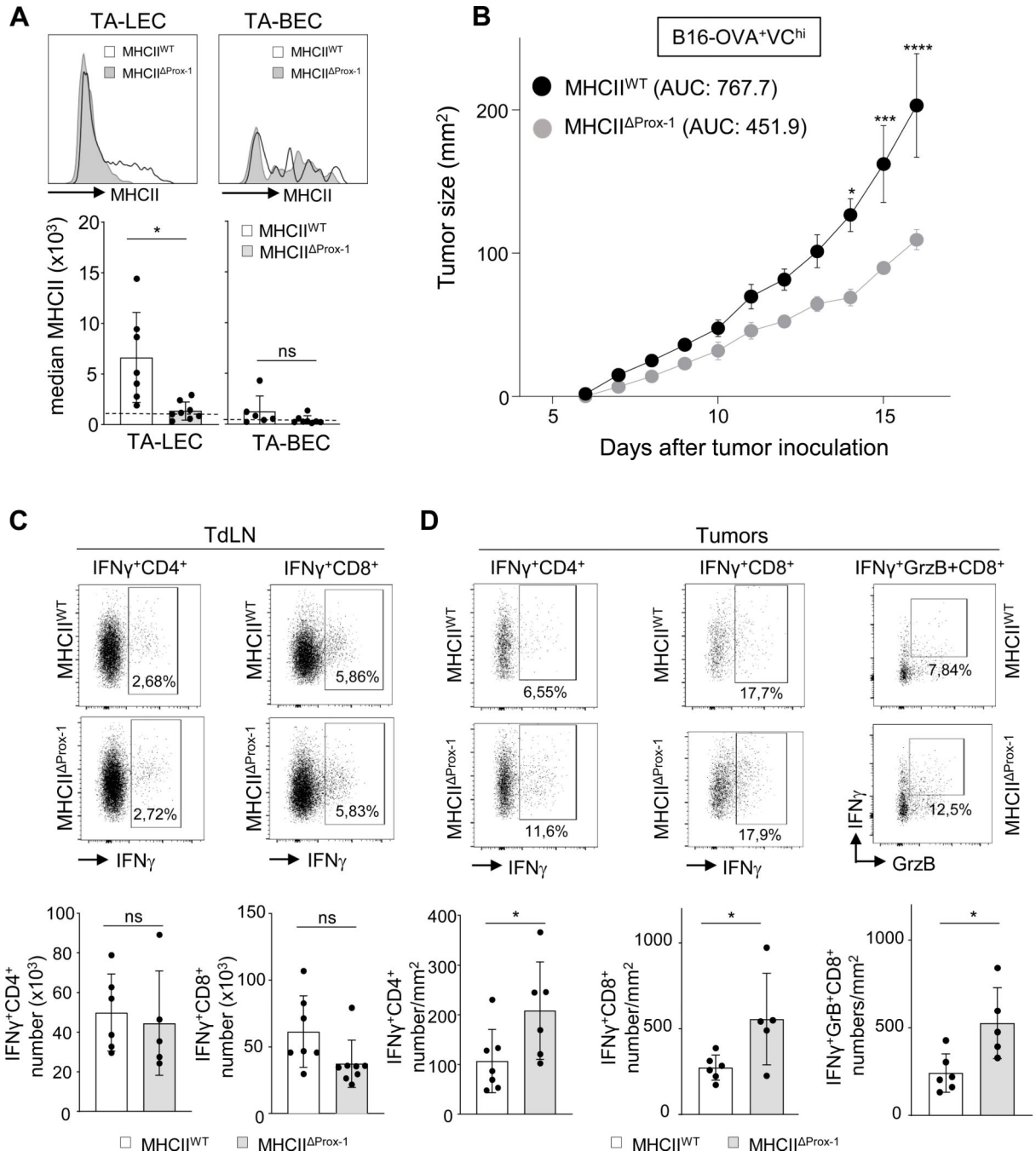

Figure 2. Impaired lymphangiogenic B16-OVA^{+}VC^{hi} tumor growth and enhanced tumor infiltrating T cell effectors in absence of MHCII expression by LECs.

(A-D) Tamoxifen-treated MHCII$^{\Delta Prox-1}$ and MHCII^{WT} mice were injected with B16-OVA^{+}VC^{hi} cells. (A) FACS histogram representative examples and quantification of MHCII expression by LECs and BECs at day 12 in tumors. (B) Tumors were measured every day. Area under the curve (AUC) is provided. (C) Representative flow cytometry dot plots and absolute numbers of IFNγ-producing CD4^{+} T cells and IFNγ-producing CD8^{+} T cells in TdLN at day 12. (D) Representative flow cytometry dot plots and densities (absolute numbers/mm^{2}) of IFNγ-producing CD4^{+} T cells, IFNγ-producing, and Granzyme

B (GrB)+IFNγ-producing $CD8^+$ T cells in tumors at day 12. Data are representative of 3 independent experiments with 7–9 mice per group. Error bars represent mean ± SD. (A, C, D) un-paired, non-parametric t-test, (B) Two-way ANOVA. *p <0.05; **p < 0.01; ***p < 0.001.

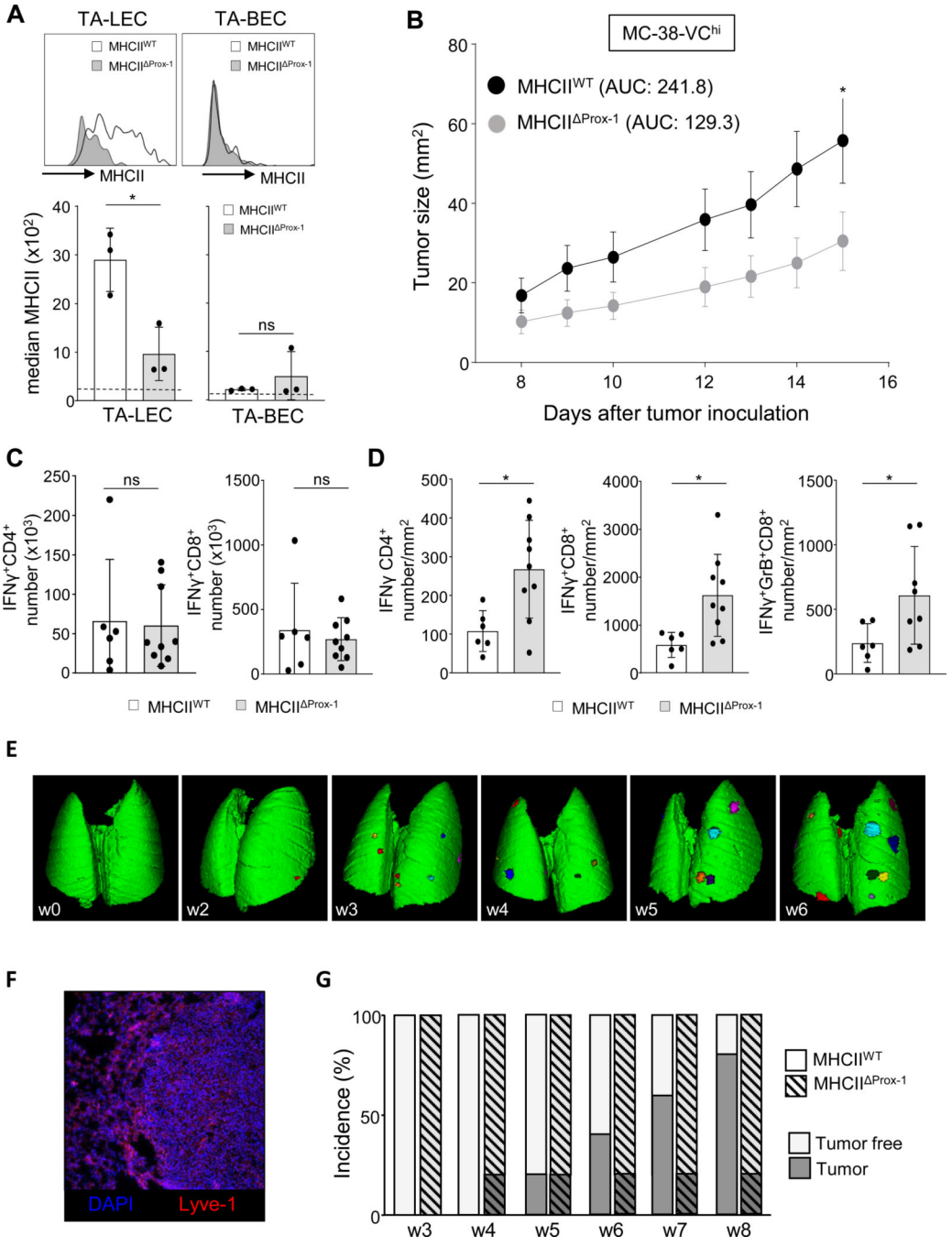

Figure 3. Absence of MHCII expression by LECs impairs lymphangiogenic tumor growth, enhances tumor infiltrating T cell effectors in MC-38-VC^{hi} tumors and affects lung adenocarcinoma tumor incidence.

(A-D) Tamoxifen-treated MHCII$^{\Delta Prox-1}$ and MHCII^{WT} mice were injected with MC-38-VC^{hi} cells. (A) FACS histogram representative examples and quantification of MHCII expression by LECs and BECs at day 15 in tumors. (B) Tumors were measured every 1–2 days. (C) Absolute numbers of IFNγ-producing CD4$^+$ T cells and IFNγ-producing CD8$^+$ T cells in TdLN at day 22. (D) Densities (absolute numbers/mm^2) of IFNγ-producing CD4$^+$ T cells, IFNγ-producing, and Granzyme B (GrB)+IFNγ-producing CD8$^+$ T cells in tumors

at day 22. Data are representative of 2 independent experiments with 6 mice per group. **(E-G)** Murine lung adenocarcinoma $Kras^{-/-}p53^{-/-}$ tumor cells were injected i.v. in C57BL/6 mice (E, F) and tamoxifen-treated $MHCII^{WT}$ and $MHCII^{\Delta Prox-1}$ mice (G). (E) Lung X-ray Computed Tomography scans (0–6 weeks, "w"). Tumor nodules were arbitrarily coloured. (F) 5 μm section of lung tumor nodule area stained for Lyve-1 (LECs, red) and DAPI (blue) at week 4. (G) Tumor incidence were followed in $MHCII^{WT}$ and $MHCII^{\Delta Prox-1}$ mice as in (e). Results represent the tumor incidence. One experiment, 5 mice / group. Error bars represent mean ± SD. (A, C, D) un-paired, non-parametric t-test, (B) Two-way ANOVA. *p <0.05; **p < 0.01; ***p < 0.001.

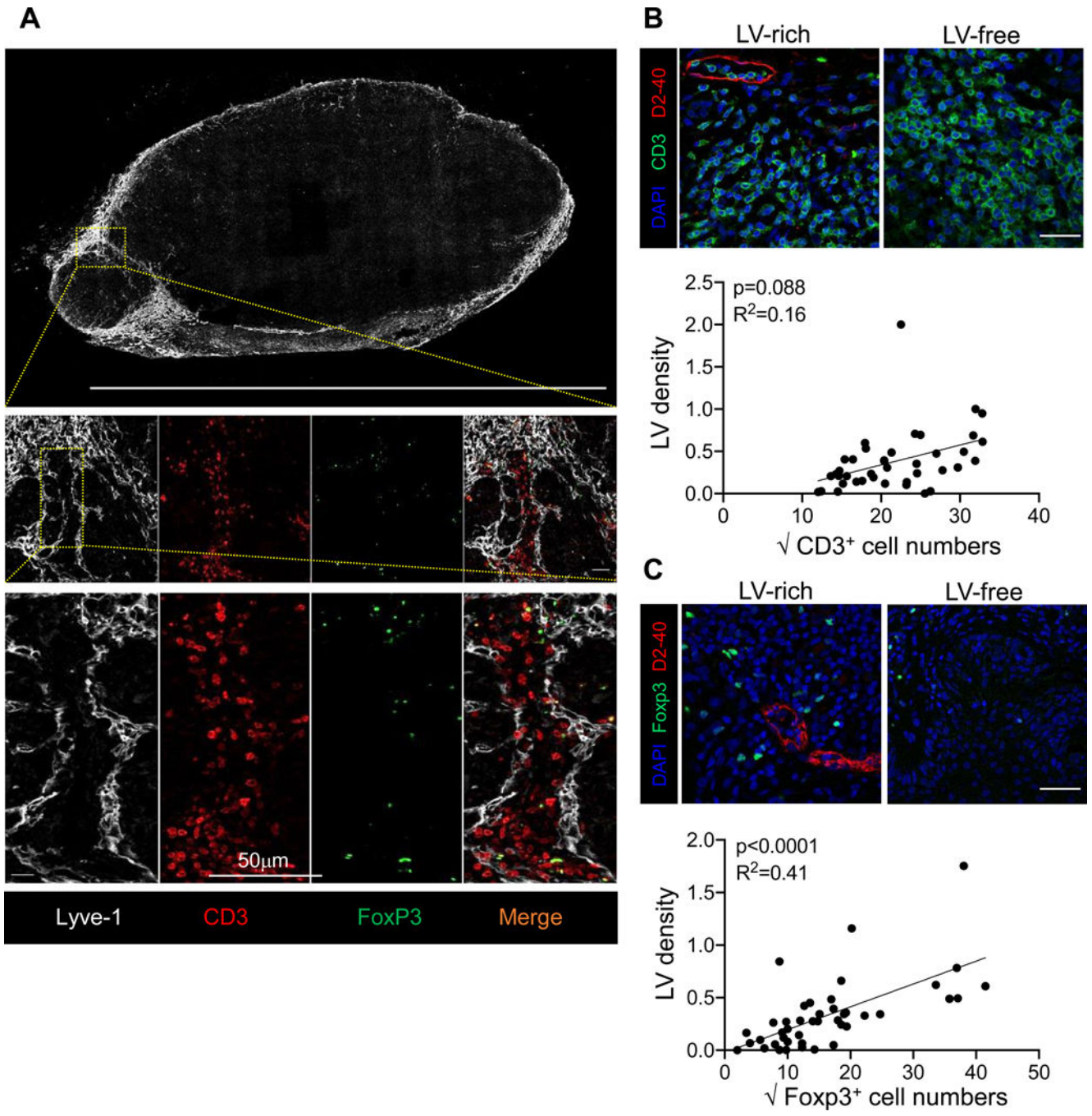

Figure 4. FoxP3^{+} T cells accumulate around lymphatics in VEGF-C overexpressing tumors.

(A) C57BL/6 mice were injected with B16-OVA^{+}VC^{hi} tumor cells. Montages of maximum projected 3D confocal images acquired by SDCM of a representative melanoma section immunostained for LVs (Lyve-1, grey), T cells (CD3, red), Tregs (Foxp3, green). Images were obtained using a 10x (top row) or a 40x (middle, bottom row) objective including a 3x relative magnification in the bottom row. Selected regions of interest are indicated by dashed squares and denote magnified areas shown in lower images. Scale bars 1 cm (top), 50 μm (middle) and 20 μm (bottom). **(B, C)** Human melanoma sections (from 6 melanoma

samples) depicting (B) LECs (D2–40, red) and total T cells (CD3, green) or (C) LECs (D2–40, red) and Tregs (Foxp3, green) in lymphatic vessel rich (LV-rich) and lymphatic vessel free areas (LV-free) (DAPI, blue). Scale bars 10 μm. Graph shows the correlation between LV density ($D2–40^+$, % of total area) and the amount of T cell density ($CD3^+$cells/mm2) (B) or Treg density ($Foxp3^+$cells/mm^2) (C).

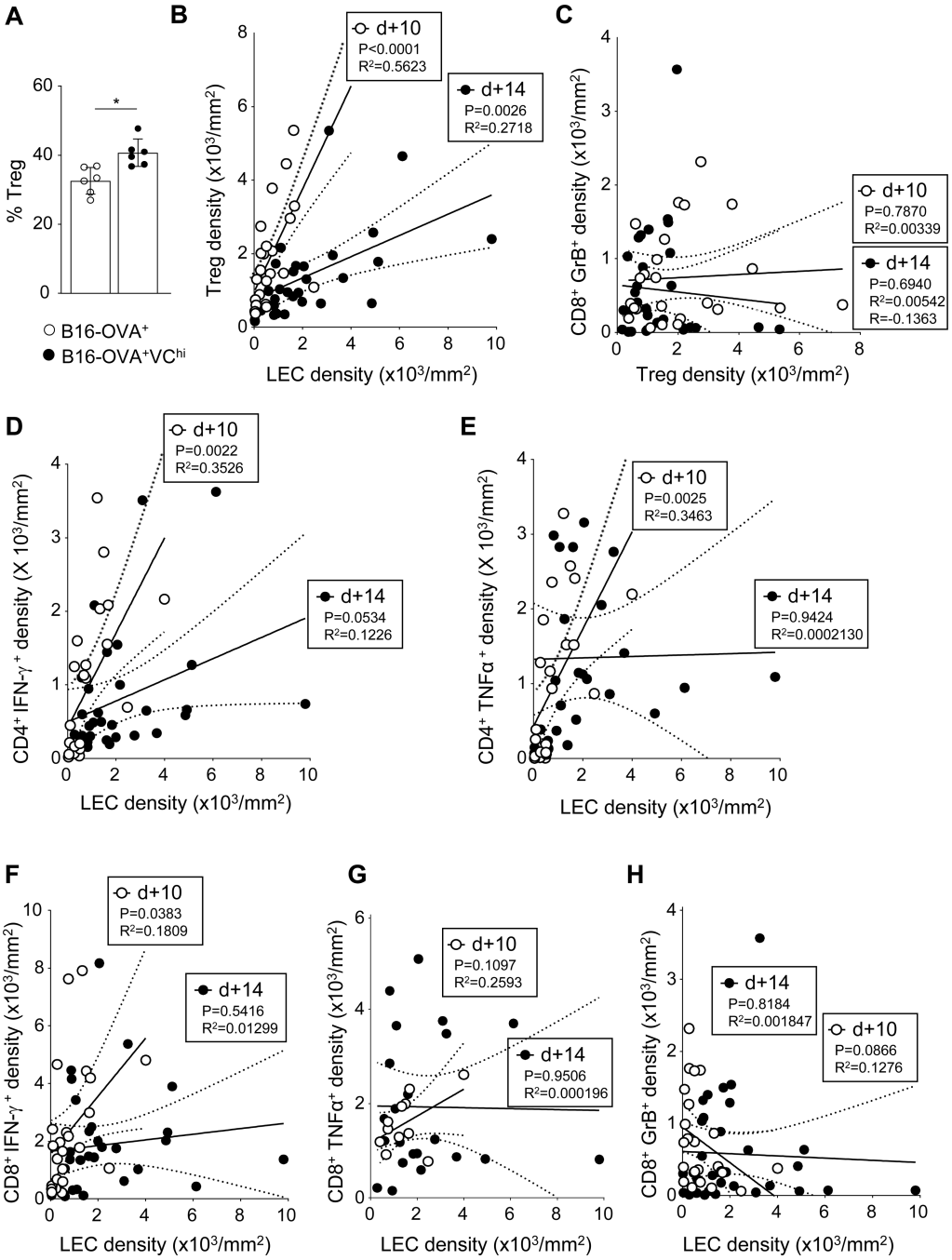

Figure 5. TA-lymphangiogenesis is correlated with enhanced tumoral Treg densities and reduced effector CD8$^+$ T cell densities.

(A-H) C57BL/6 were injected with B16-OVA$^+$ (A) or B16-OVA$^+$VC^{hi} (A-H) tumor cells. (A) Tumor-infiltrating Treg (CD25^{hi} FoxP3$^+$ cells among CD4$^+$) frequencies were evaluated at day 10. Data are representative of three independent experiments with 5–6 mice / group each. Student's t-test. *p <0.05. (B-G) Correlation graphs between (B) tumoral LEC and Treg densities, (C) tumoral Treg and GrB-producing CD8$^+$ T cell densities, (D) tumoral LEC and IFNγ producing CD4$^+$ T cell densities, (E) tumoral LEC and TNFα-producing

$CD4^+$ T cell densities, (F) tumoral LEC and IFNγ producing $CD8^+$ T cell densities, (G) tumoral LEC and TNFα-producing $CD8^+$ T cell densities and (H) tumoral LEC and GrB-producing $CD8^+$ T cell densities. Data are pooled from 2 time points (day 10 and day 14) and are pooled from 2 to 3 independent experiments with a total of 18–25 mice per group. Density is indicated as $x10^3$ /mm^2. Linear regression, *p <0.05.

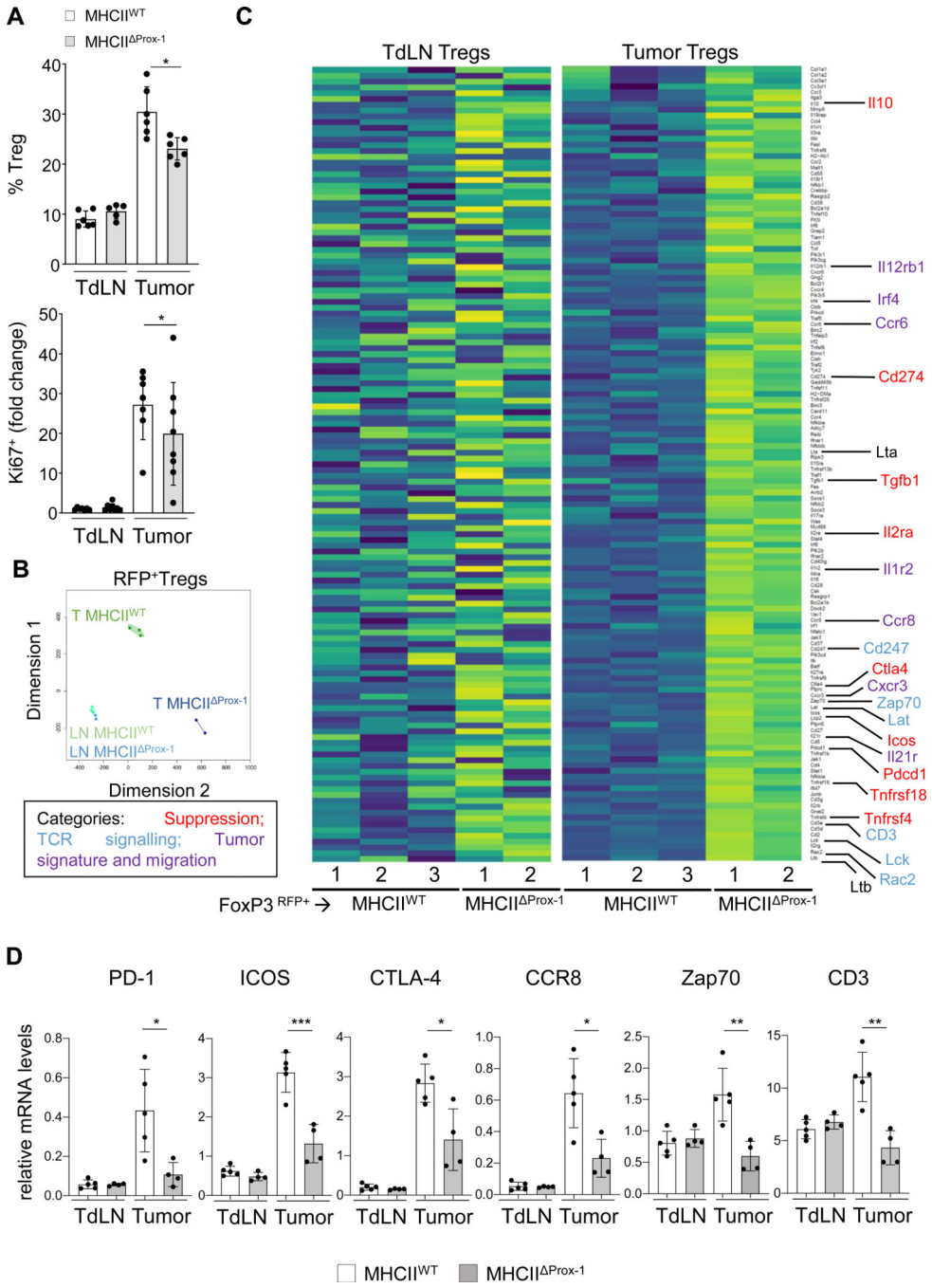

Figure 6. Lymphangiogenic tumor Treg transcriptome and phenotype are locally modulated by MHCII expression on LECs.

(A) Tamoxifen-treated MHCII$^{\Delta Prox-1}$ and MHCII^{WT} mice were injected with B16-OVA^{+}VC^{hi} tumor cells. (A) Frequency and proliferation (Ki67^{+}) of Foxp3^{+} Tregs were assessed in TdLNs and tumors at day 12 by flow cytometry. Data are representative of 3 experiments with 8 mice per group. Error bars represent mean ± SD. Un-paired, non-parametric t-test, **p <0.01. **(B-D)** Tamoxifen-treated Foxp3^{RFP}RORγt^{GFP}→MHCII$^{\Delta Prox-1}$ and Foxp3^{RFP}RORγt^{GFP}→MHCII^{WT} mice were injected with B16-OVA^{+}VC^{hi} cells.

Foxp3^{RFP} cells were purified by flow cytometry from TdLN and tumors at day 12. (B) Multi-dimensional-scaling analysis ("T", tumor; "LN", TdLN). (C) Gene expression analysis was performed by RNA-seq (2–3 replicates per condition). Heatmaps with z-score showing genes sorted for immunological relevance from GSEA list of upregulated pathways. Genes that belong to indicated pathways are color-coded. (D) mRNA expression levels of indicated genes measured by qPCR. Data are pooled from 4–5 mice per group. Error bars represent mean ± SD. Student's t-test, *p <0.05; **p < 0.01; ***p < 0.001.

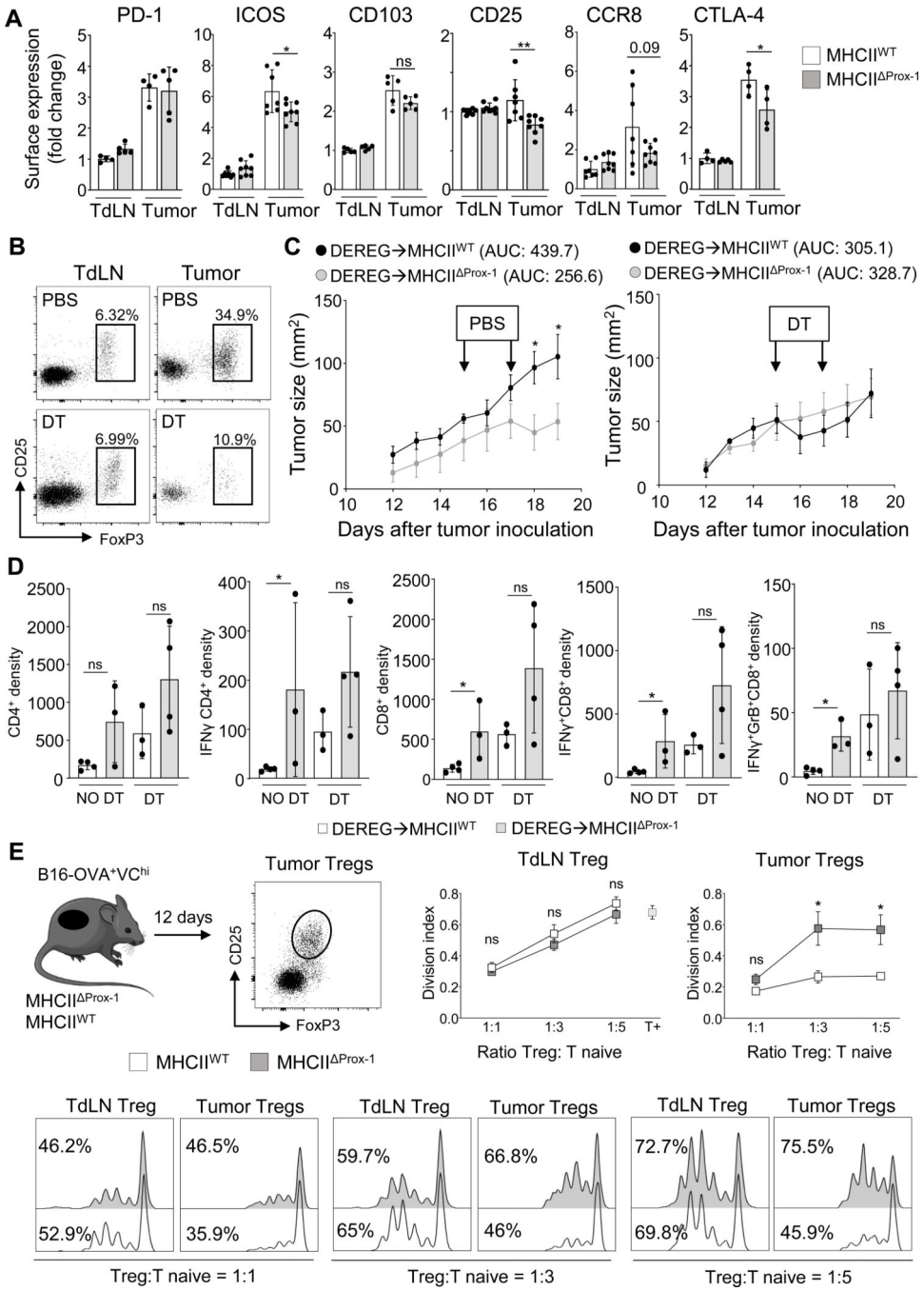

Figure 7. MHCII expression by tumor LECs promotes impaired intratumoral Treg suppressive functions.

(A) Tamoxifen-treated MHCII$^{\Delta Prox-1}$ and MHCII^{WT} mice were injected with B16-OVA^{+}VC^{hi} cells, and the expression level of indicated markers was assessed on Tregs (gated on CD4^{+}Foxp3^{+}CD25^{hi} cells) by flow cytometry in TdLN and tumors at day 12. Histograms represent levels of expression (median) for each marker. Data are representative of 3 experiments with 4–8 mice per group. Error bars represent mean ± SD. **(B-D)** Tamoxifen-treated DEREG→MHCII^{WT} and DEREG→MHCII$^{\Delta Prox-1}$ BM chimeras were

injected with B16-OVA^{+}VC^{hi} cells. DT was injected intratumorally at indicated time points (black arrows). (B) FACS dot plot showing an example of Foxp3^{+}CD25^{hi} Treg frequencies among CD4^{+} T cells in tumors at day 19 after tumor inoculation in untreated or DT treated MHCII^{WT} mice. (C) Tumor growth was followed at indicated time points in non-treated mice (left) (SEM: MHCII^{WT} 105.25±17.695, MHCII$^{\Delta Prox-1}$ 53.68±14.41) and DT treated mice (right) (SEM: MHCII^{WT} 72.13±19, MHCII$^{\Delta Prox-1}$ 69.47±14.35). (D) Densities (absolute numbers/mm^2) of IFNγ-producing CD4^{+} T cells and IFNγ-producing or Granzyme B (GrB) + IFNγ-producing CD8^{+} T cells in tumors at day 19. Data are representative of 2 experiments with 3–5 mice per group. Error bars represent mean ± SD. Student's t-test, *p <0.05; **p < 0.01. **(E)** Tamoxifen-treated MHCII$^{\Delta Prox-1}$ and MHCII^{WT} mice were injected with B16-OVA^{+}VC^{hi} cells and CD4^{+}CD25^{hi} cells were sorted from tumors and TdLNs after 12 days, and cultured at indicated ratio with CFSE-labelled CD4^{+}CD25^{neg} stimulated with anti-CD3 antibodies and BMDCs. Experimental design for Treg FACS sort, FACS histograms show the proliferation of naïve T cells after 3 days (the frequency of dividing cells is indicated), and division index of CFSE-labelled T cells. Data are pooled from one experiment with a total of 16 mice / group, (4 mice pooled / sample). Error bars represent mean ± SD. (A, D) un-paired, non-parametric t-test, (C, E) Two-way ANOVA. *p <0.05; **p < 0.01; ***p < 0.001.